Recent advances in design of hierarchically porous Fe1-Nx-C based electrocatalysts for zinc-air batteries

DIAMOND RELATED MATERIALS

Jinyi Chen, Hanieh Akbari, Hong Zhang, Dan J.L. Brett, Jian Guo, Srinivas Gadipelli

PII: S0925-9635(24)00896-3

DOI: https://doi.org/10.1016/j.diamond.2024.111683

Reference: DIAMAT 111683

To appear in: Diamond & Related Materials

Received date: 5 June 2024

Revised date: 2 October 2024

Accepted date: 18 October 2024

Please cite this article as: J. Chen, H. Akbari, H. Zhang, et al., Recent advances in design of hierarchically porous Fe1-Nx-C based electrocatalysts for zinc-air batteries, *Diamond & Related Materials* (2024), https://doi.org/10.1016/j.diamond.2024.111683

This is a PDF file of an article that has undergone enhancements after acceptance, such as the addition of a cover page and metadata, and formatting for readability, but it is not yet the definitive version of record. This version will undergo additional copyediting, typesetting and review before it is published in its final form, but we are providing this version to give early visibility of the article. Please note that, during the production process, errors may be discovered which could affect the content, and all legal disclaimers that apply to the journal pertain.

© 2024 Published by Elsevier B.V.

Recent advances in design of hierarchically porous Fe₁-N_x-C based electrocatalysts for zinc-air batteries

Jinyi Chen, Hanieh Akbari, Hong Zhang, Dan J. L. Brett, Jian Guo, at and Srinivas Gadipelli^{a,c}*

^cElectrochemical Innovation Lab, Department of Chemical Engineering, University College London, London, WC1E 7JE, UK.

E-mail: jianguo@scu.edu.cn (JG); s.gadipelli@ucl.ac.uk (SG)

Abstract

Zinc-air batteries with high theoretical energy density, earth-abundant raw materials, ecofriendliness and safety are considered as promising next generation energy devices. Their commercial advancement can be boosted with the development of inexpensive and high-performing oxygen reduction reaction (ORR) catalysts. The precious platinum-group metal-based nanoparticles dispersed in conducting carbon black (e.g., Pt/C) are the typical ORR catalysts. The iron-nitrogen-carbon-based materials, specifically comprising atomic-level iron-nitrogen coordination in hierarchical porous carbon support (usually denoted as Fe₁-N_x-C), have shown promising electrocatalytic activities by delivering important half-wave and on-set potentials and reduction current densities along with high durability due to the favorable adsorptive and reduction ability of Fe₁-N_x centers for molecular oxygen in alkaline electrolyte. Numerous studies have been focused on rational design of the hierarchically porous structures to enhance the accessibility of active Fe₁-N_x sites and mass-transfer characteristics for efficient oxygen reduction and intermediate species. Therefore, in this review, several design strategies relevant to the template and self-template synthesis routes for hierarchically porous Fe₁-N_x-C catalysts are insightfully presented. A detailed discussion is offered on the ORR activity and performance of Fe₁-N_x-C catalysts in zinc-air batteries. Further opportunities and challenges for the rational design and application of Fe₁-N_x-C catalysts are also discussed.

Keywords: Synthesis strategies; hierarchical porous structures; Fe₁-N_x-C; oxygen reduction reaction; single-atom electrocatalysts; zinc-air batteries

^aCollege of Physics, Sichuan University, Chengdu, 610064 China.

^bDepartment of Physics and Astronomy, University College London, London, WC1E 6BT, UK

^{*} Corresponding authors.

1. Introduction

Research on the efficient clean energy technologies has attracted a considerable attention due to growing concerns with the greenhouse gases, e.g., carbon dioxide, emissions (also known as carbon emissions) from the combustion of conventional fossil fuels for the energy generation.^[1–5] Among the various forms of clean or low-carbon emission energy conversion and storage processes, such as hydrogen and renewables of solar and wind, the electrochemically energy technologies, which include batteries, fuel cells and supercapacitors, have shown promising efficiencies and prospects.^[3,4] The metal-air batteries, in particular, aqueous zinc-air batteries are attractive owing to their high theoretical energy density (1218 Wh kg⁻¹, compared to <350 Wh kg⁻¹ of lithium-ion batteries), environmental friendliness and excellent safety compared to organic electrolyte-based lithium-ion batteries.^[6,7] In addition, zinc-air batteries are relatively inexpensive due to the earth-abundance of zinc anode and use of alkaline electrolyte.^[8]

Unlike ion-intercalation and deintercalation in rechargeable lithium-ion batteries, the rechargeable zinc-air batteries operation relies on the oxygen reduction reaction (ORR) and oxygen evolution reaction (OER) – both of which occurs on the air cathode comprising catalyst materials. [9,10] However, high-performing catalyst is required to promote the ORR, which is a complex and sluggish process involving multiple electron transfers and various intermediate species and thus, inevitably leads to slow cathode kinetics. [11,12] Nowadays, the common commercial catalysts used for ORR are platinum-based nanoparticles dispersed on conducting carbon black (Pt/C) catalysts. [11-13] Although Pt/C-based catalysts exhibit high activity, their low ORR stability along with low abundance and high cost limiting their large-scale commercial application. [4,14] Therefore, there is a requirement for the development of high-performing and durable non-precious metal-based ORR catalysts. [3,15-17]

Nitrogen-doped carbon materials have shown high ORR catalytic activity, because they can lead to an unbalanced internal charge distribution. [18-21] Furthermore, the atomically dispersed metal centers in nitrogen-doped nanoporous carbon (M₁-N_x-C; where M₁ can be Pt₁, Fe₁, Mn₁, Co₁, Mo₁ and Pd₁) type class has emerged as most promising catalysts due to their maximum atom utilization efficiency, tunable coordination structures and optimal active components. [22-25] Related studies have confirmed that nitrogen-doped porous carbon can change the charge density and spin density of carbon atoms, which can greatly enhance the anchoring ability of metal sites. [26] The M-N_x sites formed by metal atoms and coordinated N atoms in carbon substrate are the key factors for high activity of the catalyst. [27,28] These sites favor oxygen adsorption and intermediate desorption effectively to promote the ORR. [29] Among the M₁-N_x-C family of catalyst materials, the Fe₁-N_x-C structure offered ORR catalytic performance on par with or superior to Pt/C. However, the ORR relevant metrics, such as on-set and half-wave reduction potentials, reduction current density and electron and mass transfer reactions are primarily dependent on the Fe₁-N_x site coordination, stability and concentration, along with porous and conductive characteristics of the substrate nanoporous carbon matrix.

Therefore, these systems pose challenges in designing and delivering desirable ORR activity and zinc-air battery performance. [27,30–32]

To obtain optimal electrochemical reaction condition in the three-phase boundary region that comprising gas (O2, the reactant)-liquid (electrolyte, the medium/product)-solid (catalyst, the air cathode), the common method is to increase the number of active sites embedded in the accessible porous carbon skeleton, which also facilitates the mass transport of reactants/intermediates/products. [33,34] Micropores in the catalyst materials host the majority of active sites, and mesopores/macropores can favor for mass transfer reactions. [35,36] It is generally accepted that the metal atoms/centers are the ORR active sites. [37] Therefore, the selection of a suitable metal center is crucial. In 2011, for the first time, it was shown that single Pt atomic dispersion in ultra-low concentrations on FeO_x substrate (Pt₁/FeO_x) can offer higher oxidizing activity in thermochemical conversion of CO oxidation compared to typical nanoparticle-based Pt/FeO_x. [38] Since then, the research on single metal atomic catalysts has attracted tremendous attention^[4,39]. In case of electrocatalysis, it has been shown that Fe₁ is the most effective central metal atom among the transition metal-based M₁-N_x-C catalysis for efficient ORR reaction. [39,40] However, it has been also identified that these M₁ centers are very susceptible to agglomeration due to their extremely high surface energy. [41] Such characteristic property of M₁-N_x-C-based materials can greatly affect both the catalytic activity and durability of ORR. To prevent the migration and aggregation of single metal atoms, the selection of a suitable carbon support becomes essential. The strong interaction between the support and the metal atoms serves to stabilize the metal centers. [42,43] Carbon-based materials are commonly used supports/substrates for the electrochemical applications due to their highly tunable physicochemical properties, such as high electrical conductivity, chemical stability and chemical reactivity for the production of porous structures and/or heterogeneous surfaces with metallic and non-metallic dopants.^[44] The rational design of the porous carbon support structures is key to enhance overall activity of the catalyst. [45] Hierarchically porous and heteroatom doped carbons with large specific surface area have offered impressive activities, as the pores (especially mesopores) allow faster access of the electrolyte to the active sites and ensure effective contact between electrolyte and electrode surface. During electrochemical reactions, volume changes in the carbon matrix can be accommodated by the mesopores, which helps to limit structural degradation and catalytic performance degradation during long-term cycling operation. [46,47] The modulation of space geometry can adjust the electronic properties and electrical conductivity of the carbon-based materials. [48] Therefore, constructing carbon supports with 3-dimensional (3D) hierarchical porous structures is an effective and mainstream design strategy.[49]

This review discusses recent progress on the rational design of hierarchically porous carbon-based atomically dispersed Fe_1 - N_x -C relevant electrocatalysts for ORR and relevant zinc-air batteries. Advancements in the various forms of synthesis strategies involving templates or self-templates are classified and summarized. The electrochemical processes and the advantages of hierarchical porous structures for ORR in zinc-air

batteries are described. Important insights and perspectives on the further development of hierarchically porous M_1 - N_x -C catalysts for zinc-air battery are also discussed to accelerate commercial application process of both catalysts and metal-air batteries.

2. Fundamental knowledge of rechargeable zinc-air battery

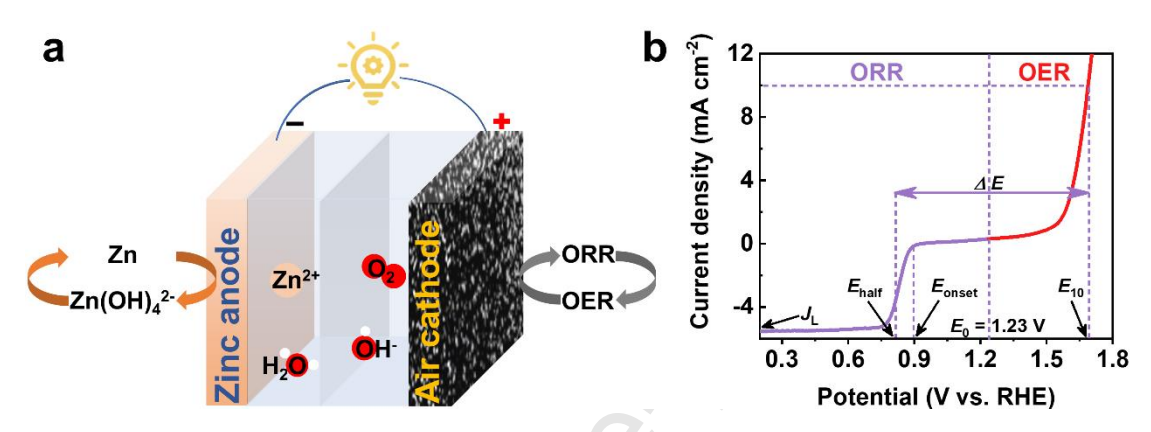


Figure 1. a) Schematic of rechargeable zinc-air battery. Electrocatalyst on the air cathode accelerates the reaction rates of ORR and OER. [50,51] b) Typical OER and ORR voltammetric curves.

As shown in **Figure 1a**, a standard rechargeable zinc-air battery comprises zinc metal anode and catalyst cathode with separator immersed in the aqueous electrolyte. [52–60] The separator is used as a barrier to prevent short circuits caused by direct contact between the cathode and the anode. The battery works by means of a redox reactions between cathode and anode to achieve charging and discharging. [61] During the charging/discharging process, oxidation of electrolyte and reduction of oxygen occurs at catalyst and are usually associated with OER and ORR, respectively (**Figure 1a**). During the discharge process in the alkaline medium, O_2 at the three-phase interface (which is gas-liquid and solid interface of oxygen, electrolyte and electrode) is converted to hydroxide ions according to Eq. (1). The hydroxide ions migrate to zinc anode and react with metallic zinc to form $Zn(OH)_4^{2-}$ (Eq. (2)). When $Zn(OH)_4^{2-}$ is supersaturated, it decomposes into ZnO (Eq. (3)). Accordingly, the overall discharge reaction is represented by Eq. (4).

Air electrode:
$$O_2 + 4e^- + 2H_2O \rightarrow 4OH^-$$
 (1)

Zinc electrode: $Zn + 4OH^- \rightarrow Zn(OH)_4^{2-} + 2e^-$ (2)

 $Zn(OH)_4^{2-} \rightarrow ZnO + H_2O + 2OH^-$ (3)

Overall reaction: 2Zn +
$$O_2 \rightarrow 2ZnO$$
 (4)

During the charging, a reverse reaction of the discharge reaction takes place at air electrode; where OER reaction occurs, and oxygen is evolved from the hydroxide ions in the alkaline electrolyte (Eq. (5)). At the zinc electrode, ZnO is reduced to metallic Zn and deposited on zinc electrode (Eq. (6)-(7)). The relevant overall charge reaction is governed by Eq. (8).

Air electrode:
$$4OH^{-} \rightarrow O_{2} + 2H_{2}O + 4e^{-}$$
 (5)

Zinc electrode: $ZnO + H_{2}O + 2OH^{-} \rightarrow Zn(OH)_{4}^{2-}$ (6)

 $Zn(OH)_{4}^{2-} + 2e^{-} \rightarrow Zn + 4OH^{-}$ (7)

Overall reaction: $2ZnO \rightarrow 2Zn + O_{2}$ (8)

Moreover, ORR usually proceeds via two reaction pathways of two-electron ($2e^-$) and four-electron ($4e^-$) transfer steps. Here, $4e^-$ pathway (Eq. (9)) facilitates a direct reduction of oxygen to hydroxide ions, whereas, $2e^-$ (Eq. (10)-(11)) reaction favors the intermediate product formation of hydrogen peroxide, which is corrosive and tends to enable oxidative reactions from active O* species of peroxide, $^{[62]}$ and is far less efficient than the $4e^-$ process. $^{[63]}$ In ORR, both pathways normally occur together and the number of electrons transferred during the reaction can be calculated to determine the dominant ORR pathway. As shown in **Figure 1b**, the ORR electrocatalytic activity is usually assessed by the half-wave potential (E_{half} or $E_{1/2}$) and the onset potential (E_{onset}), which is defined as the potential on the linear sweep voltammetry (LSV) test graphs at a current density of 0.1 mA cm⁻². E_{half} is the potential on the LSV curve at half the diffusion-limiting current density. Material stability can be measured by accelerated durability test and chronoamperometric response. E_{onset}

Four-electron process (alkaline conditions):

$$O_2$$
 + $2H_2O$ + $4e^ \rightarrow$ $4OH^-$ (9)

Two different two-electron processes (alkaline conditions):

$$O_2$$
 + H_2O + $2e^ \rightarrow$ OOH^- + OH^- (10)
 OOH^- + H_2O + $2e^ \rightarrow$ $3OH^-$

(11)

Like ORR, the OER reaction (Eq. (12)) mechanism is complex and accompanied by multi-step electron transport processes^[67]. Generally, starting with the coordination between the active metal sites attached to the catalyst surface and the hydroxide ions and culminating in the development of molecular oxygen. The overpotential is an important parameter for evaluating the catalytic performance of OER (**Figure 1b**). The overpotential is usually defined as the difference between the potential measured at 10 mA cm⁻² or 100 mA cm⁻² and the theoretical water dissociation thermodynamic potential of 1.23 V. The Tafel slope in the Tafel diagram is also a parameter for evaluating the performance of OER and ORR. Tafel diagrams reveal the relationship between overpotential and current density, the equation is $\eta = a + b*logj$, where b is the slope, the lower the slope the better the catalytic activity, this also applies to the performance of ORR.

OER:
$$4OH^- \rightarrow O_2 + 2H_2O + 4e^-$$
(12)

3. Design strategies of hierarchically porous Fe₁-N_x-C based ORR catalysts and their application in zinc-air batteries

Tremendous efforts have been focused on the rational design and production of hierarchically porous Fe_1 - N_x -C structures with high performing ORR activity and the further application in zinc-air batteries. Generally, the synthesis strategies of hierarchically porous Fe_1 - N_x -C materials mainly include template and self-template (template-free) routes. These methods, in turn, have their own subcategories. For example, the template methods can be subdivided into hard and soft-templates, and the self-template method can be similarly categorized into template-free metal-organic frameworks (MOFs), covalent-organic frameworks (COFs) and supramolecular-based derivatives and biomass-derivative. As shown in **Figure 2**, their relevant synthesis strategies with relevant advantages and disadvantages are described in this section.

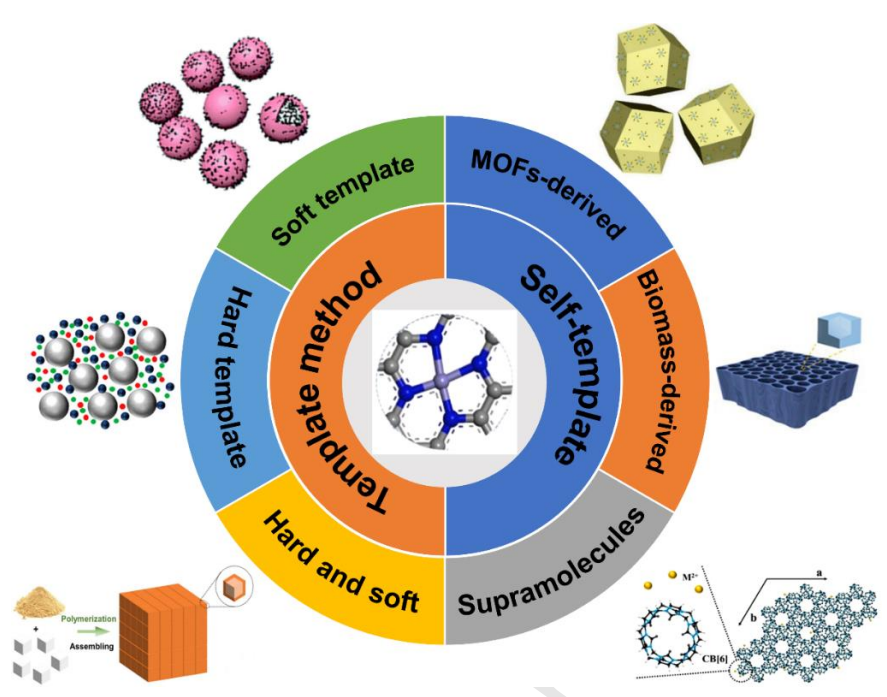


Figure 2. Overview of the topics covered in this review with schematic illustration of the design strategies for hierarchically porous Fe_1 - N_x -C based materials. [80,95,96,110,120,131,142] ([80]] Reproduced with permission. Copyrights (2020), Royal Society of Chemistry; [95]] Reproduced with permission. Copyrights (2018), John Wiley and Sons; [96]] Reproduced with permission. Copyrights (2022), Elsevier; [110]] Reproduced with permission. Copyrights (2022), Elsevier; [120]] Reproduced with permission. Copyrights (2023), John Wiley and Sons; [142]] Reproduced with permission. Copyrights (2021), Elsevier)

3.1 Template methods

The template methods are the most often used strategies for constructing hierarchically porous nanostructured materials. Depending on the physicochemical characteristics of the templates, this can be divided into soft- and hard-template methods. Hard-templates are materials with well-defined shapes, e.g., silicon dioxide (SiO₂), zinc oxide (ZnO), magnesium oxide (MgO) and sodium chloride (NaCl), ^[68–70] while soft-templates are usually decomposable self-assembled surfactants and amphiphilic block copolymers,

e.g., F127, polyvinylpyrrolidone (PVP), and inorganic metal-coordinated molecular structures.^[71–73]

3.1.1 Soft-templates

As presented in **Figure 3**, the soft-template methods have the advantages of being convenient, cheap, and environmentally green for the preparation of hierarchically porous materials. The soft-templates with functional groups can turn into micelles, which then self-sacrifices during the carbonization process and becomes a source for backbone carbon support to build porous materials and also often introduces heteroatom dopants

into the resultant carbon structures. [74] The pore size of the mesoporous carbon can be adjusted by controlling the self-assembly of the soft micelles. However, what hinders the widespread use of the soft-templating strategy is the weak interaction between the surfactant and the carbon precursor, where the surfactant micelles are often expelled from the polymer during the soft-template polymerization process.^[75,76] Mesoporous carbon nanospheres (MCNSs) with high surface area and pore size facilitates the enhancement of mass transport for ORR. [77] Based on a simple acid-assisted organicorganic self-assembly approach, Wei et al.[78] synthesized homogeneous MCNSs by direct hydrothermal treatment of phenol-formaldehyde solution and triblock copolymer plurnonic F127 under acidic conditions (2M HCI), followed by carbonization treatment. By knowing that CO_2 at high temperatures can etch the carbon framework (C + $CO_2 \rightarrow CO$ + C_{porous}) for the formation of highly microporous carbon, which can enhance the accessibility of the ORR active sites, [79] Hao et al. [80] prepared Fe₁-N_x-C type MF-C-Fe-Phen-800 catalyst by pyrolyzing the melamine-formaldehyde (MF) resin spheres templated carbon black with FeCl₃ and 1,10-Phenanthroline (Fe-Phen) additives, as depicted step-by-step in Figure 3a. In the process, MF generates CO2 during high temperature pyrolysis that promotes the further formation of microporous carbon structure.

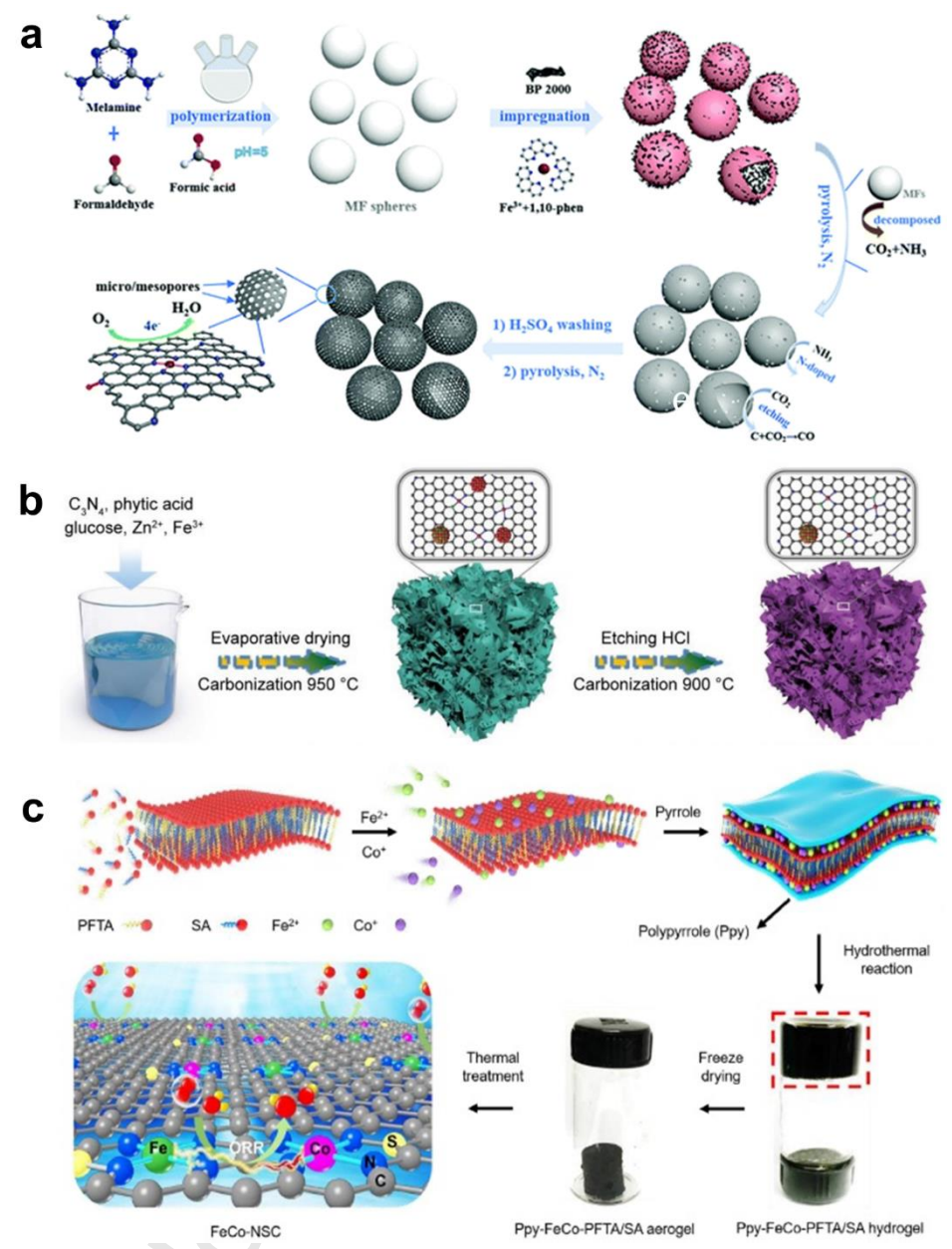


Figure 3. a) Schematic illustration of soft-template design process (MF nanospheres were synthesized via a polymerization process and used as template, then, the MF nanospheres were coated with BP2000 and Fe-Phen compounds followed by pyrolysis, acidic washing and second pyrolysis). [80] (Reproduced with permission. Copyrights (2020), Royal Society of Chemistry) b) Schematic preparation of FePNC via metal-coordinated polymerization of C_3N_4 , phytic acid and glucose with Fe³⁺ and Zn²⁺ precursors followed by pyrolysis and acid washing and second pyrolysis. [81] (Reproduced with permission. Copyrights (2023), John Wiley and Sons) c) Schematic illustration procedure for FeCo-NSC via pyrolysis of hydrothermally generated aerogel of pyrrole polymerized lamellar micelle structure formed by PFTA and SA with Fe³⁺ and Co²⁺ ions. [82] (Reproduced with permission. Copyrights (2022), Elsevier)

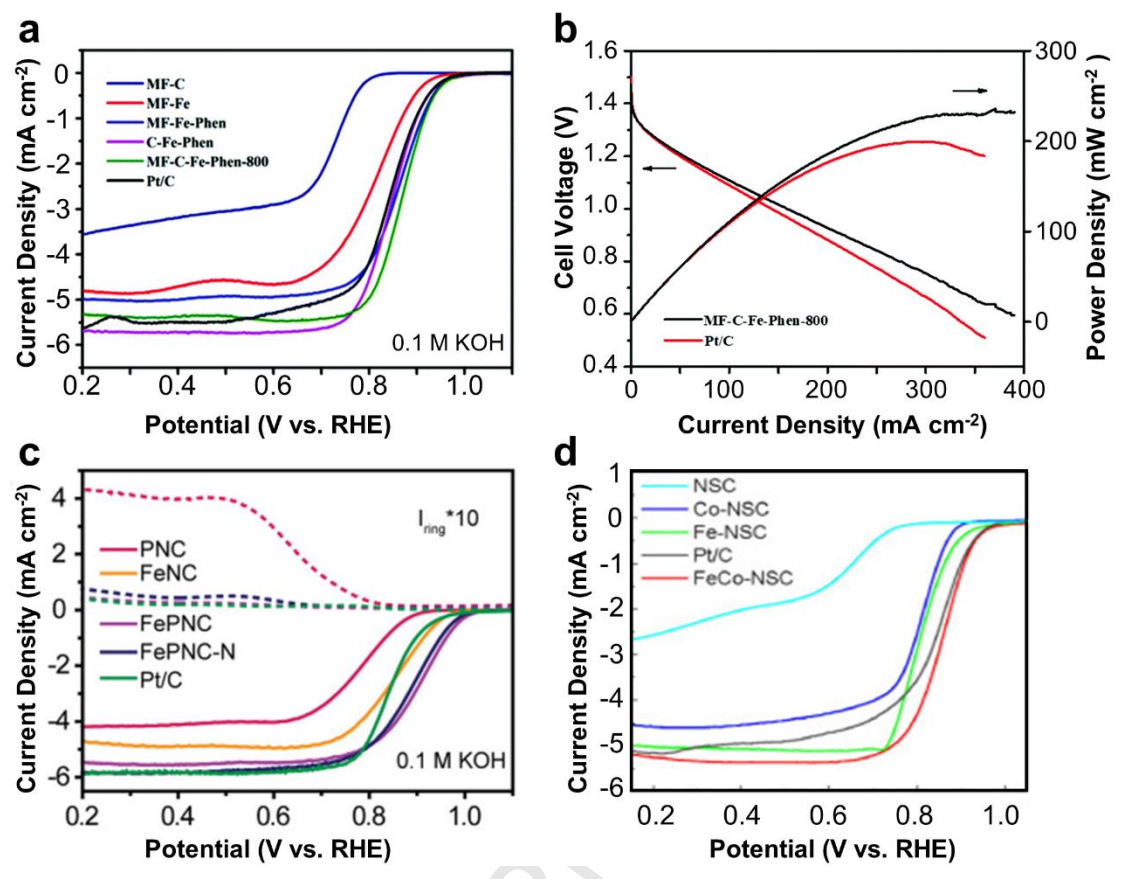


Figure 4. a) ORR LSV curves of MF-C, MF-Fe, MF-Fe-Phen, C-Fe-Phen, MF-C-Fe-Phen-800 and Pt/C in O₂-saturated 0.1 M KOH solution. [80] (Reproduced with permission. Copyrights (2020), Royal Society of Chemistry) b) Discharge polarization curves and corresponding power density curves of zinc—air batteries with MF-C-Fe-Phen-800 and Pt/C as the cathodes. [80] (Reproduced with permission. Copyrights (2020), Royal Society of Chemistry) c) ORR LSV curves for the resultant catalysts and Pt/C in 0.1 M KOH. [81] (Reproduced with permission. Copyrights (2023), John Wiley and Sons) d) ORR LSV curves of FeCo-NSC, Fe-NSC, Co-NSC, NSC and Pt/C in O₂-saturated 0.1 M KOH. [82] (Reproduced with permission. Copyrights (2022), Elsevier) All the LSV curves were recorded at a rotating speed of 1600 rpm.

In Liu et al. research, [81] the layered carbon nitride (C_3N_4) with phytic acid was used as a soft-template that self-sacrifice along with phosphorus doping to generate asymmetric N, P-coordinated Fe₁ sites (Fe₁-P/N-C). Briefly, C_3N_4 pre-synthesized by direct pyrolysis of urea was first dispersed into methanol solution containing phytic acid, and then a certain amount of glucose and metal salts (Fe, Zn) were added to the above solution, and finally carbonized after evaporation and drying. The resulting carbonized solid was acid washed to leach out the zinc and excess Fe-nanoparticles and subjected to further secondary pyrolysis to obtain the catalyst (**Figure 3b**). Dual-metal single-atom catalysts have been shown to have several advantages compared to single-metal catalysts due to the synergistic action of neighboring metal atoms. [83,84,85] However, dual-metal single-atom based catalysts synthesis requires carefully controlled design strategy to stabilize them on the carbon support. [86,87] Therefore, the construction of a more stable supports

required to enhance the utilization of metal atoms for the efficient catalytic performance. A 2D atomic layers sheet-like soft-template was prepared by Wu et al. via self-assembly of two kinds of amphiphiles, perfluorotetradecanoic acid (PFTA) and stearic acid (SA) into a lamellar micelle. This template served to confine metal ions between layers as well as to build a porous structure for synthesis of dual-metal single-atom FeCo-NSC catalyst (**Figure 3c**).

As shown in Figure 4, these as-synthesized Fe₁-N_x-C type catalyst materials described above have shown to yield high catalytic performance for ORR as presented by linear sweep voltammogram (LSV) curves. For example, Fe-N/MCNSs catalysts offered excellent stability and resistance to methanol under alkaline conditions. The MF-C-Fe-Phen-800 catalyst with a high specific surface area of 807 m² g⁻¹, exhibited E_{1/2} of 0.87 V in 0.1 M KOH solutions (Figure 4a). Zinc-air battery with this catalyst delivered superior power density of 235 mW cm⁻² at a high current density of 371 mA cm⁻² (Figure 4b) with high open circuit voltage of 1.65 V, compared to Pt/C catalyst. Recent studies have shown that disrupting the symmetric electron distribution of Fe₁ sites can effectively enhance the intrinsic activity of the ORR reaction. [88] The relevant Fe₁-P/N_x-C catalyst outperformed the Pt/C by delivering the $E_{1/2}$ of 0.90 V (in 0.1 M KOH) as shown in **Figure 4c**. Moreover, the $E_{1/2}$ of the FeCo-NSC is 0.86 V (**Figure 4d**), superior to that of NSC (0.63 V), Fe-NSC (0.81 V), Co-NSC (0.80 V) and even better than commercial Pt/C (0.85 V). Besides, the FeCo-NSC showed the highest diffusion-limiting current density (J_L) of 5.26 mA cm⁻² among the studied catalysts. Moreover, Zhang et al. developed a general route to synthesis M₁-N_x-C via formamide condensation and carbonization; the assynthesized single-atom electrocatalyst with dense atomically dispersed FeN₃–CoN₃ sites showed excellent ORR activity and stability. [39]

3.1.2 Hard-templates

The hard-templates can effectively generate well-defined hierarchical porous structures with the post-synthesis removal of macro- or mesoscopic solid hard-templates. During the synthesis, these templates added to the carbonaceous precursors, mixed and solidified and then removed by dissolving in strong acids/bases, while leaving the equivalent size nanocavities to produce well-defined porous carbon structures, also called ordered porous carbons. For example, silica (SiO₂)-based hard-templates have been used commercially and are relatively mature templates due to their simplicity of preparation and chemical/thermal stability. The core-shell structure is a model structure frequently used. This structure is attributed to preventing the aggregation of metal centers.

3.1.2.1 Silica-based

Silica is widely used template as a shell material.^[90] Liao et al. prepared Fe₁-N_x-C type Fe-N-HMC hierarchical porous carbon electrocatalyst using a core-shell approach.^[91] A high nitrogen content-based core-shell precursor was synthesized by mixing silica template with melamine monomer of tripolycyanamide (TCA) and paraformaldehyde,

followed by Fe³⁺ addition and heat treatment produced Fe-N-HMC (Figure 5a). The synthesized material has a honeycomb porous structure, which is advantageous for further exposure of catalytically active sites and has a potential for large-scale applications due to its low cost and facile synthesis. Zhao et al. [92] prepared hierarchically macroscopic bimodal 3D carbon interwoven nanorod-type networks containing high concentration of Fe₁ active sites (Fe/RNC) by melting and pyrolyzing the precursors with porous silicon nanorods (Figure 5b). Furthermore, Wu et al. used silica nanospheres (NKM-5) to construct hierarchically porous Fe₁-N_x-C via nanoconfined pyrolysis method. [93] The NKM-5 template and the complexation of Fe/Zn-(Methyllmidazole)₂ process creates a spherical-type material with a porous structure after carbonization followed by template removal. This synthesis offered high nitrogen dopant concentration in carbon framework and can preventing the aggregation of Fe₁-atoms. The electrochemical study results show improved mass transfer reactions with such catalyst. For example, as shown in Figure 6a, Fe/N/C-HP exhibited excellent ORR activity with E_{1/2} of 0.9 V in alkaline solution. The primary zinc-air battery constructed with Fe/N/C-HP as cathode catalyst exhibited an open circuit voltage of 1.484 V, which was 46 mV higher compared to commercial Pt/C catalyst. The discharge polarization curves of battery showed a maximum power density of 181 mW cm⁻², which was also higher than Pt/Cbased battery (Figure 6b). Likewise, ORR performance with $E_{1/2}$ of 0.856V, E_{onset} of 0.942V were attained from Fe-N-HMC catalyst (Figure 6c). [91] Fe/RNC with high level of porous network structure comprising Fe₁ concentration of 5.69 wt% and specific surface area of 739 m² g⁻¹ resulted in power density of 159 mW cm⁻² (**Figure 6d**). [92]

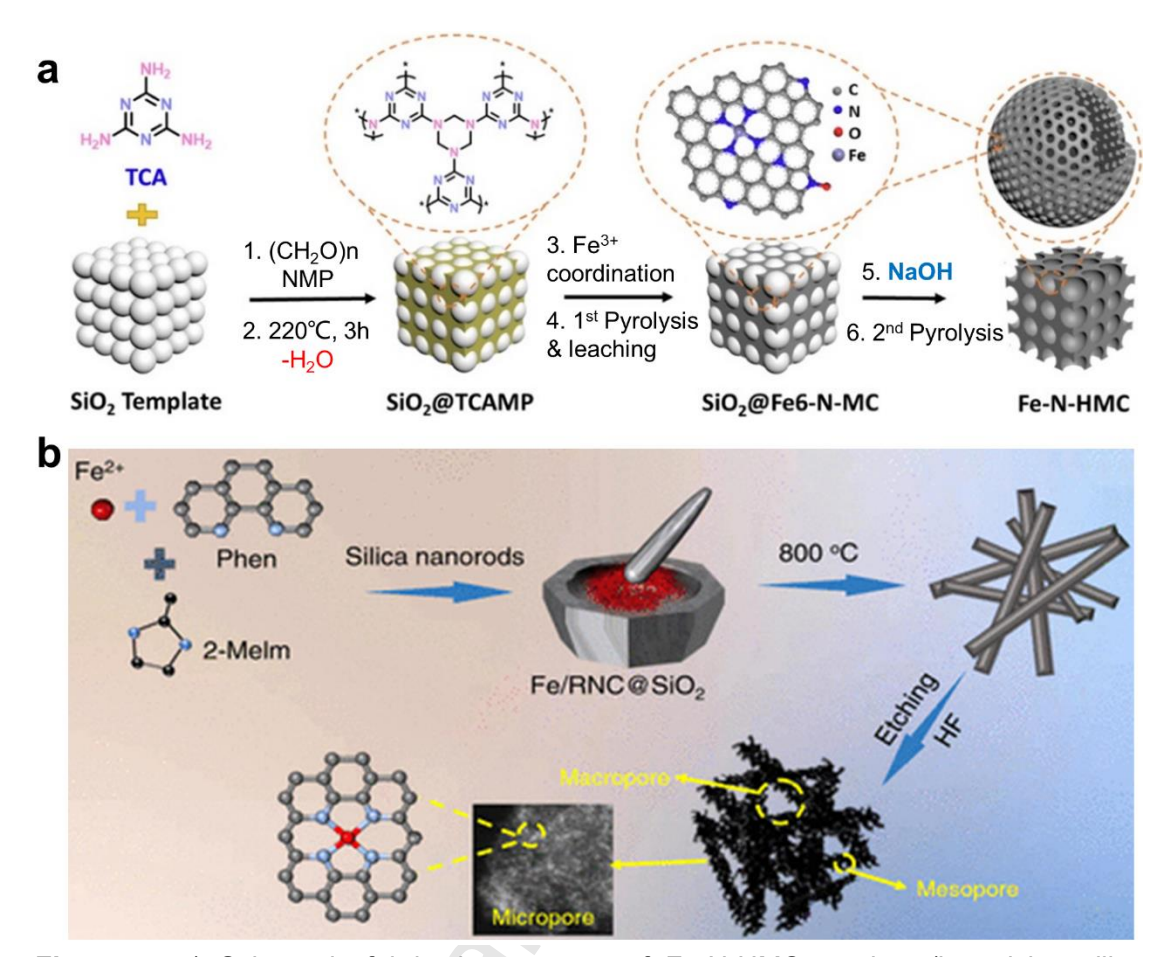


Figure 5. a) Schematic fabrication process of Fe-N-HMC catalyst (by mixing silica templates with melamine monomer (TCA=tripolycyanamide-based) and paraformaldehyde at low temperature (220 °C). Then Fe³⁺ was introduced for thermal decomposition, and the catalytic material was obtained after etching with strong alkali and further pyrolysis). [91] (Reproduced with permission. Copyrights (2023), Elsevier) b) Schematic preparation of Fe/RNC 3D nanorod network (silicon nanorods were mixed with iron and phenanthroline and dimethylimidazole by grinding, then the mixture was pyrolyzed at 800 °C, the solid was washed by strong acid (HF) to obtain Fe₁ sites in carbon matrix). [92] (Reproduced with permission. Copyrights (2022), American Chemical Society)

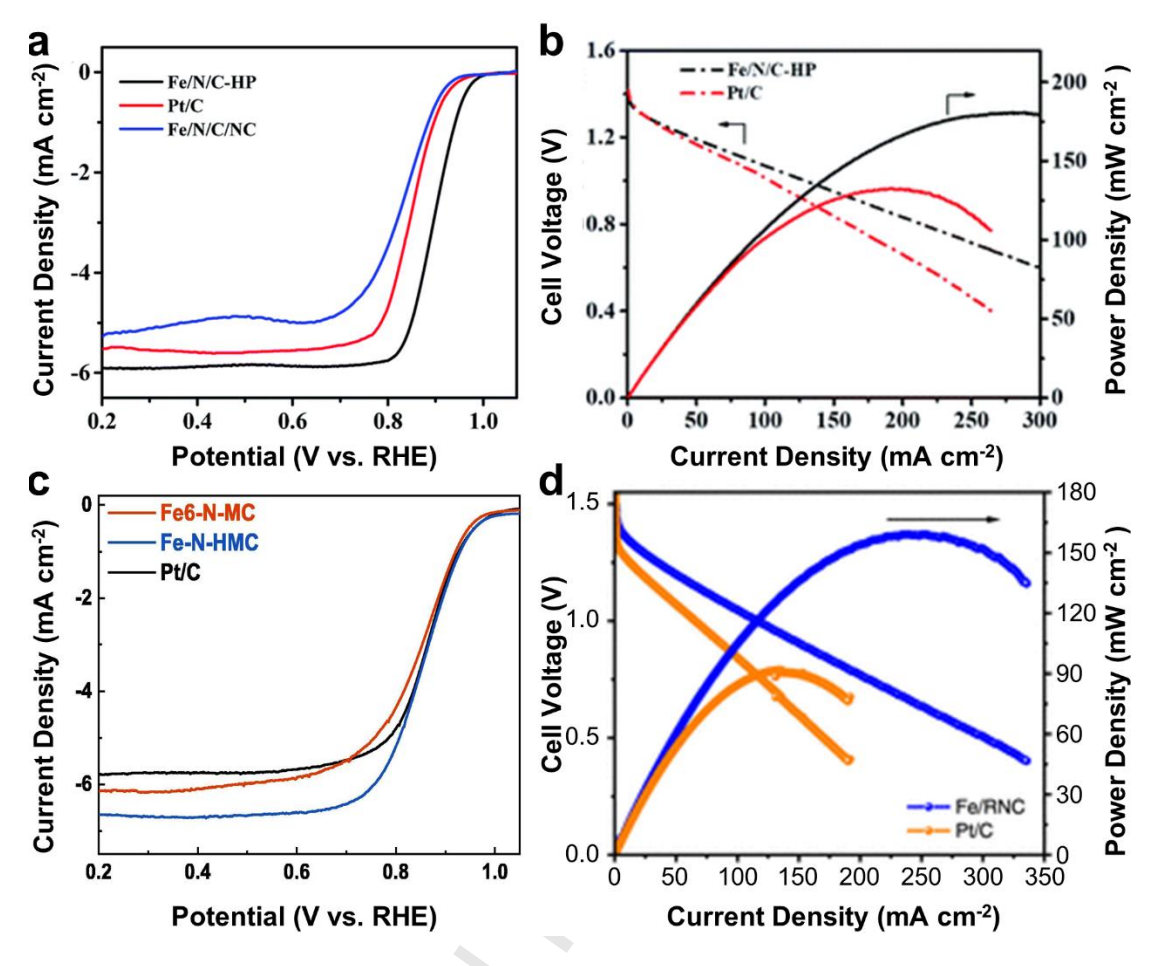


Figure 6. a) ORR LSV curves of Fe/N/C-HP, Fe/N/C/NC and Pt/C recorded in O₂-saturated 0.1 M KOH solution with a rotation rate of 1600 rpm.^[93] (Reproduced with permission. Copyrights (2020), Royal Society of Chemistry) b) Discharge polarization curves of zinc–air batteries using Fe/N/C-HP and Pt/C as cathodes.^[93] (Reproduced with permission. Copyrights (2020), Royal Society of Chemistry) c) ORR LSV curves of Fe-N-MC, Fe-N-HMC, and Pt/C recorded in O₂-saturated 0.1 M KOH solution with a rotation rate of 1600 rpm.^[91] (Reproduced with permission. Copyrights (2023), Elsevier) d) Polarization and power density curves for primary zinc–air batteries using Fe/RNC and Pt/C as cathodes.^[92] (Reproduced with permission. Copyrights (2022), American Chemical Society)

3.1.2.2 Melt salts

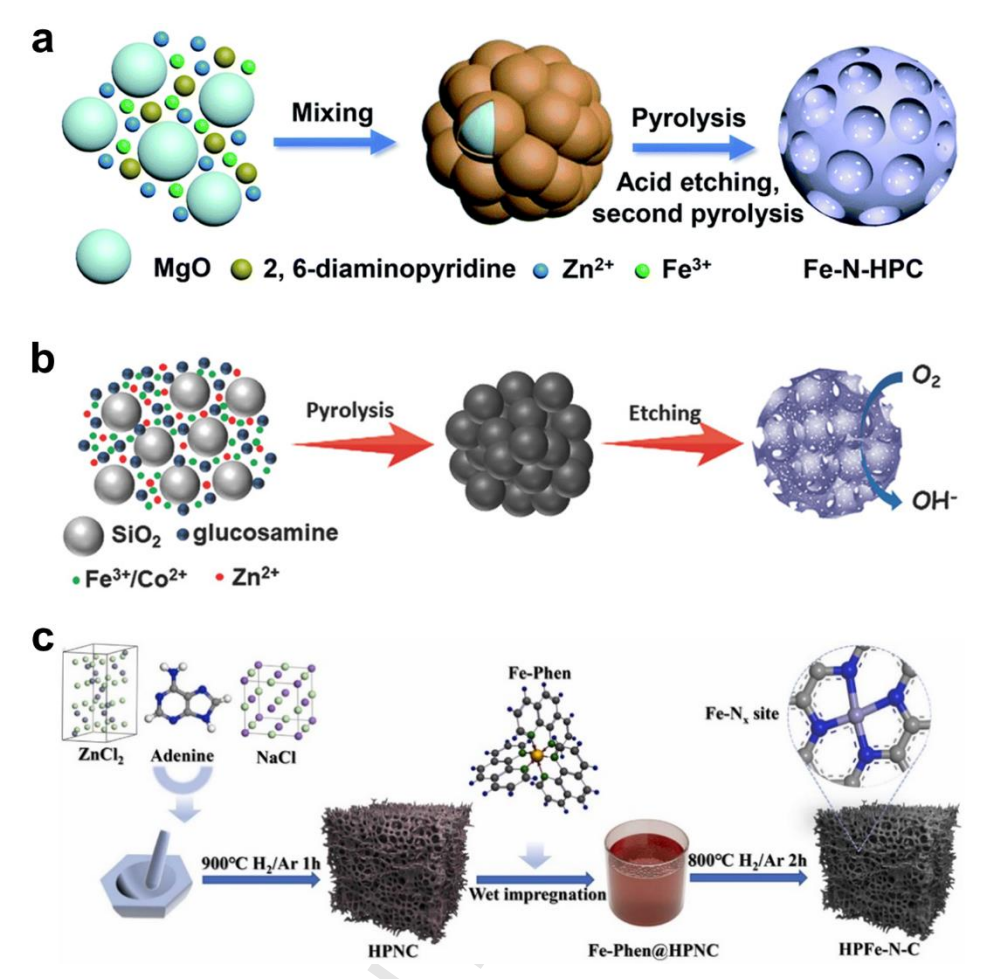


Figure 7. a) Schematic synthesis procedure of Fe-N-HPC, from 2, 6-diaminopyridine, MgO, Zn^{2^+} , and Fe^{3^+} mixture carbonization followed by acid etching and second pyrolysis. [94] (Reproduced with permission. Copyrights (2021), Royal Society of Chemistry) b) Illustration for synthesis of hierarchically porous M_1 - N_x -C (M = Co and Fe) electrocatalysts, by simply adding the SiO_2 template to glucosamine of carbon and nitrogen source and Fe^{3^+}/Co^{3^+} and Zn^{2^+} as metal and porogen/template sources, respectively, and mixture was pyrolyzed and acid etched to remove the template. [95] (Reproduced with permission. Copyrights (2018), John Wiley and Sons) c) Schematic preparation steps for HPNC and HPFe-N-C via a double salt template route; $ZnCl_2$ and $NaCl_2$ was mixed with adenine by grinding, then pyrolyzed at 900 °C, this pyrolyzed product was then wet impregnated with Fe-phenanthroline and pyrolyzed again at 800 °C to finally obtain the catalyst. [96] (Reproduced with permission. Copyrights (2022), Elsevier)

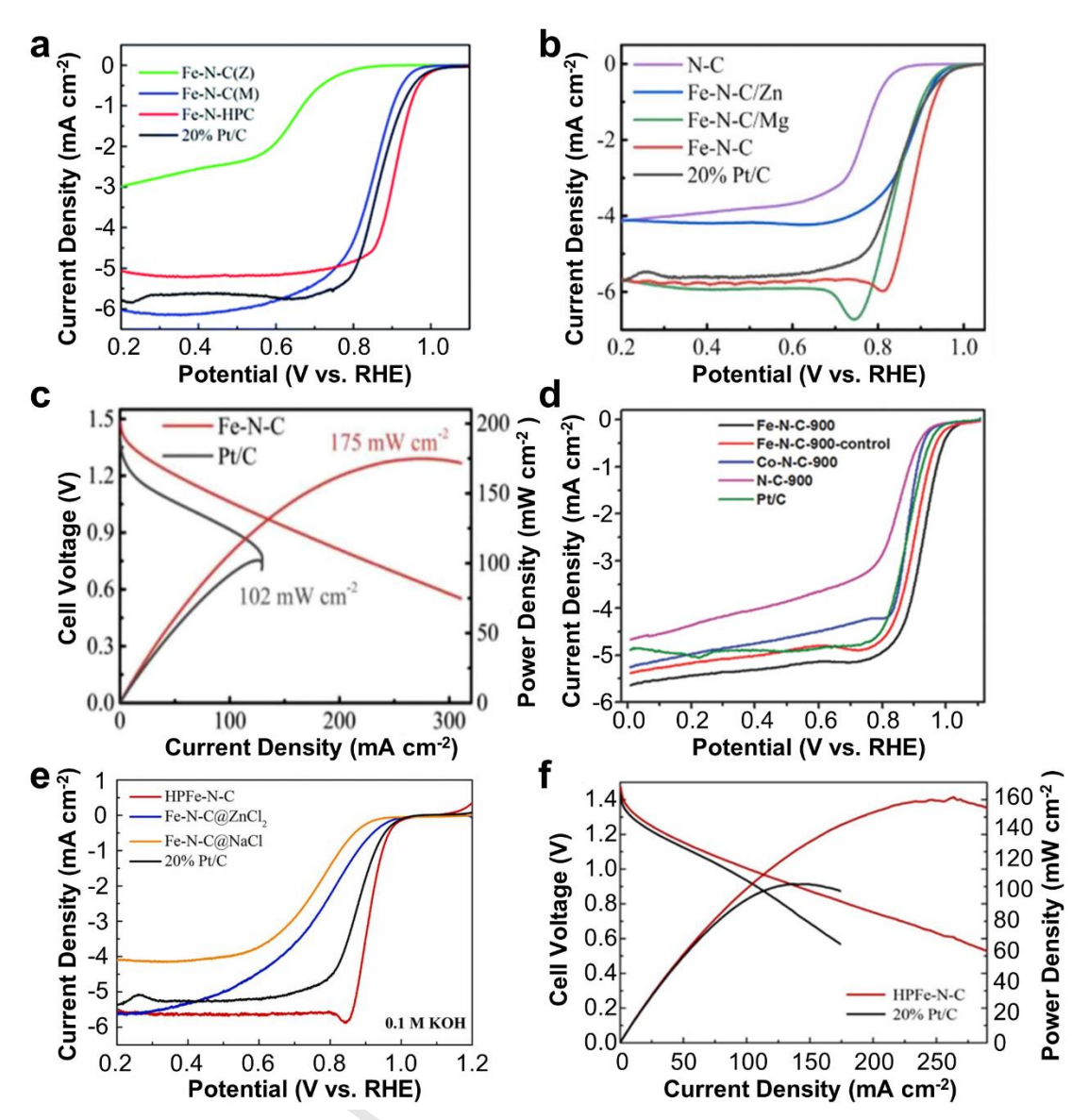


Figure 8. a-b) ORR LSV curves of Fe-N-HPC^[94] (Reproduced with permission. Copyrights (2021), Royal Society of Chemistry) (a), and Fe-N-C^[97] (Reproduced with permission. Copyrights (2022), Elsevier) (b). c) Discharge polarization and power density curves of primary zinc-air batteries using Fe-N-C and Pt/C as cathodes.^[97] (Reproduced with permission. Copyrights (2022), Elsevier) d-e) ORR LSV curves of Fe(Co)-N-C, N-C.^[95] (Reproduced with permission. Copyrights (2018), John Wiley and Sons) and HPFe-N-C^[96] (Reproduced with permission. Copyrights (2022), Elsevier) f) Discharge polarization and power density curves of zinc-air batteries using HPFe-N-C and Pt/C as cathodes.^[96] (Reproduced with permission. Copyrights (2022), Elsevier) ORR LSV curves presented were measured in O₂-saturated 0.1 M KOH electrolyte at a rotating speed of 1600 rpm.

The utilization of melt salts, especially low-melting point metal salts such as NaCl and ZnCl₂ is another usual practice in synthesis of hierarchically porous Fe₁-N_x-C materials.^[98–101] Melt salts solution is capable of breaking numerous chemical bonds of small molecular structures.^[102] The limitation of metal ion aggregation by the melt salts

makes it a unique reaction medium, particularly promising for the design of hierarchically porous Fe₁-N_x-C materials. Besides, inorganic salts are a good choice as hard-templates because of their water solubility and ease of removal/recycle. For example, ZnCl₂ has been used as an isolating agent to disperse the metal ions in the carbonaceous precursor. [94] A dual-template of ZnCl₂ and MgO mixed with Fe³⁺ species containing carbon and nitrogen source precursors, the hierarchical porous Fe-N-HPC samples with uniform Fe₁ elemental dispersion was obtained after pyrolysis following acid etching with HCl (Figure 7a). In another work, Lu et al. [97] also reported Zn-assisted MgO template strategy to construct porous Fe₁-N_x-C using PVP as source for the N-doping and carbon support. Simultaneously increasing the number of Fe₁ active sites and boosting the intrinsic activity of the active sites are effective way to construct better catalytically active materials. [103,104] It has been shown that Fe-N2 structure enable better ORR activity than Fe-N₄. [105,106] Based on this understanding, Zhu et al. [95] prepared porous Fe₁-N_x-C materials by utilizing both silica and ZnCl₂ hard-templates (Figure 7b). In addition to silica, the introduction of ZnCl₂ and glucosamine further enhanced the porosity and favored for mass transfer in ORR. The salt melts can also be effective in avoiding excessive nitrogen decomposition from the precursors while preventing the Fe-metal centers from aggregation during the pyrolysis process. [107,108] Xu et al. [96] developed a dual molten salt-mediated template method to prepare Fe₁-N_x-C catalysts with a tailored porous framework (Figure 7c). For this, ZnCl₂ and NaCl were used in combination to construct 3D porous framework. Zn evaporated during the pyrolysis process at temperature of above 907 °C and that resulted in formation of micropores, and droplets formed from NaCl melt further break down those formed micropores and ultimately produce mesopores, thus leading to desirable hierarchically porous carbon structure. Meanwhile, such double salt melts-based templates successfully blocked the spillover of N-active species and avoided their excessive loss, thus samples retained high N-doping concentration (5.21 at%).

The experimental results of Wang et al. [94] showed that the accessibility and mass transfer of the active sites of Fe₁-N_x-C catalysts were significantly improved. ZnCl₂ and MgO dual templates play a role in constructing the porous structure, thus the ORR activity was improved with $E_{1/2}$ of 0.91 V (**Figure 8a**). In the work of Lu et al. [97] the synthesized Fe₁-N_x-C material has an excellent ORR performance with E_{1/2} of 0.895 V in alkaline solution (Figure 8b). The primary zinc-air battery constructed with this catalyst exhibited a peak power density of 175 mW cm⁻² and proved to have a good stability at the same time after long charge/discharge cycle tests (Figure 8c), here, there was no significant increase in the charge/discharge voltage gap after approximately 643 h (3860 cycles) of cycling. Zhu et al. [95] work showed that their Fe₁-N_x-C material displayed higher ORR activity than Pt/C with corresponding $E_{1/2}$ of 0.927 and 0.872 V, respectively, due to its various spherical pore structures constructed through salt melt templates (Figure 8d). In the work of Xu et al. [96], HPFe-N-C materials with specific surface area of 109.86 m² g⁻¹ shown to promote mass transport while exposing Fe-N₄ sites. Furthermore, HPFe-N-C presented a much higher catalytic property with $E_{1/2}$ of 0.911 V (Figure 8e), and the assembled liquid zinc-air battery exhibited high power density of 160 mW cm⁻² (Figure 8f).



3.1.3 Combination of hard and soft-templates

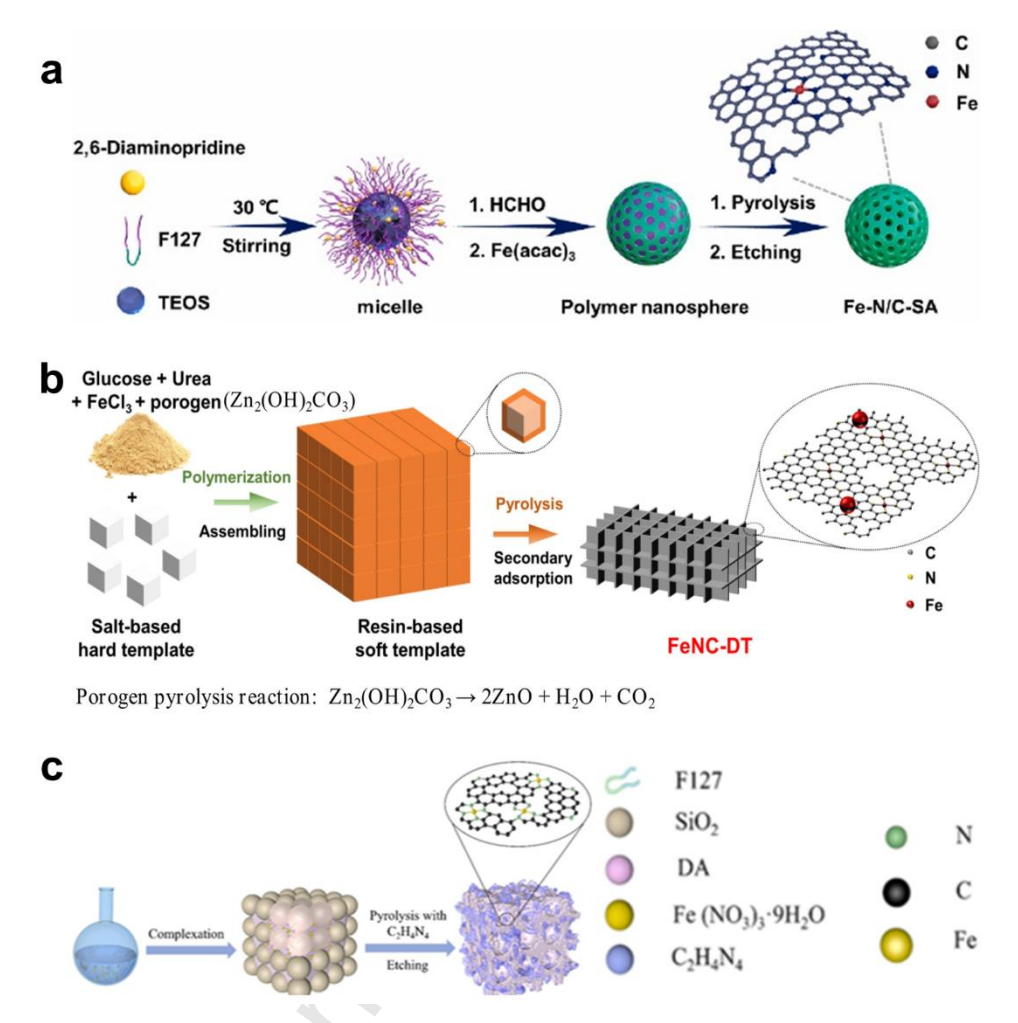


Figure 9. a) Synthetic scheme for the preparation of hierarchically porous Fe_1-N_x-C nanosphere by utilizing F127, DAP, TEOS and $Fe(acac)_3$ mixtures, which were hydrothermally treated, and products were calcined (to remove the F127 template) and carbonized at 900 °C. The resulting catalysts were then etched by HF aqueous solution (10 wt%) to remove the templates.^[109] (Reproduced with permission. Copyrights (2022), Elsevier) b) Schematic illustration of the synthetic process of FeNC-DT with the use of soft and hard-templates and precursors of glucose, urea, $FeCl_3$ and Zn^{2+} salt.^[110] (Reproduced with permission. Copyrights (2022), Elsevier) c) Synthesis strategy for DT-Fe-N-C (SiO₂ and F127 self-assembled to form micelles, then dopamine and iron nitrate were added. The mixture was allowed to crosslink and polymerize. The product was mixed with dicyandiamide by grinding and pyrolyzed at 900 °C. The template was removed by 40% HF etching).^[111] (Reproduced with permission. Copyrights (2023), Elsevier)

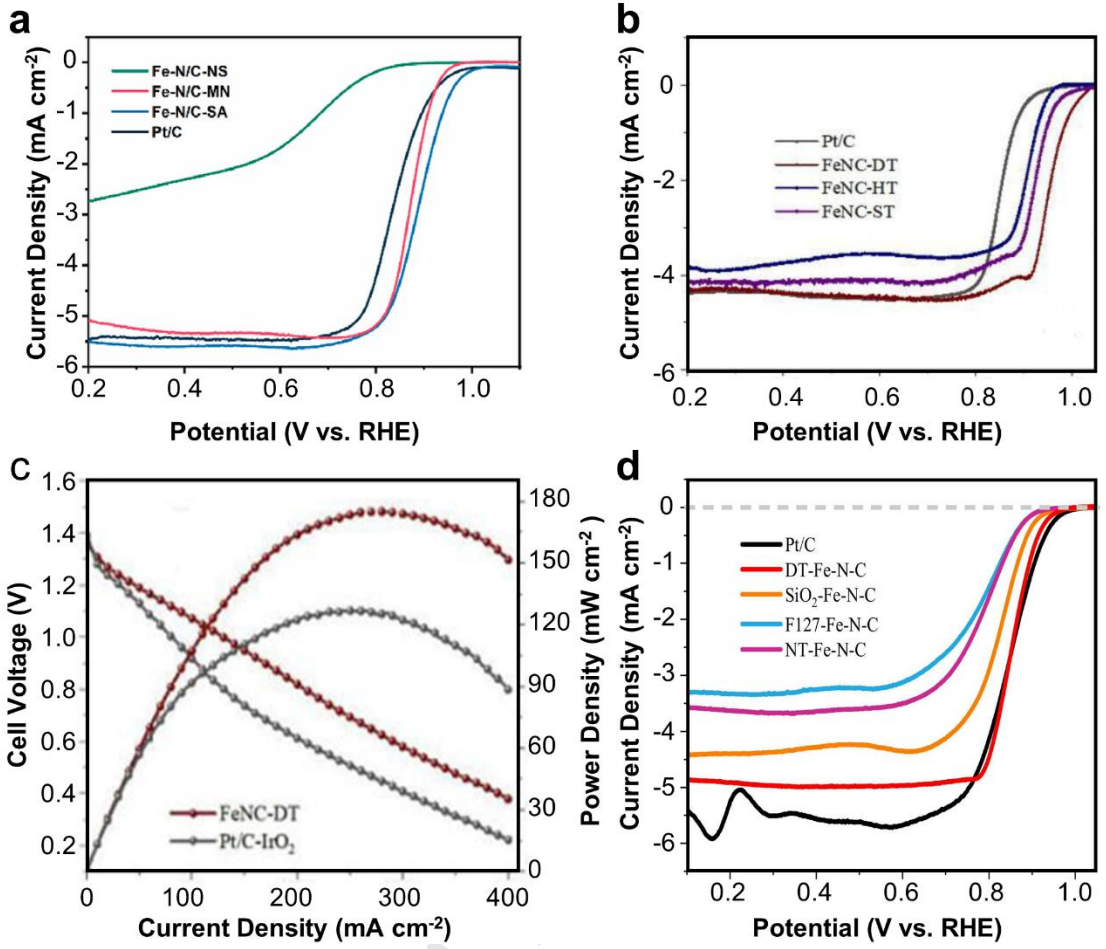


Figure 10. a) ORR LSV curves of Fe-N/C-SA.^[109] (Reproduced with permission. Copyrights (2022), Elsevier) b) ORR LSV curves of FeNC-DT, FeNC-HT, FeNC-ST and Pt/C.^[110] (Reproduced with permission. Copyrights (2022), Elsevier) c) Polarization and power density curves of the zinc–air batteries with FeNC-DT and Pt/C-IrO₂ as cathodes.^[110] (Reproduced with permission. Copyrights (2022), Elsevier) d) ORR LSV curves of DT-Fe-N-C and Pt/C.^[111] (Reproduced with permission. Copyrights (2023), Elsevier) All the LSV curves were collected at a rotation speed of 1600 rpm.

As discussed previously, soft-template methods for the preparation of hierarchical porous materials have the advantages of being convenient, inexpensive, and environmentally green, which does not require a removal process. Whereas hard-templates can effectively generate well-defined hierarchical porous structures by removing macroscopic or mesoscopic solid hard-templates after synthesis and it brings high shaping and clear pore contour size, which is easy to adjust. To make full use of the respective advantages of soft and hard-templates, the combination of soft and hard double template strategy has been employed. To expose more active sites and accelerate mass and electron transport characteristics in ORR, this method with high nitrogen-containing precursors can construct porous structures effectively. In the work of Li et al. [109], Fe₁-N_x-C materials were prepared (**Figure 9a**) by utilizing triblock polymer F127 and tetraethyl orthosilicate (TEOS) as soft and hard-templates, respectively, and 2,6-diaminopyridine (DAP) precursor was used for carbon and nitrogen source. Due to the discrete distribution of

active sites, the multi-scale porous structure is crucial for the catalytic activity of Fe₁-N_x-C catalysts. ^[112] The size continuity of different scale pores is favorable to enhance the ORR activity. ^[113] Shi et al. ^[110] work used a dual-template strategy to prepare hierarchically continuous porous FeNC-DT catalysts (**Figure 9b**). In this process, solid NaCl was used as a hard-template and a self-polymerising resin made from a mixture of urea and glucose as a soft-template, which was aimed to prevent the micro- and mesoporous structures from collapsing. Thus, as-synthesized materials exhibited a continuous porous structure. Altering the microstructure to optimize the three phase interface in the electrocatalysis can enhance the catalytic performance of the catalysts. ^[114] Accordingly, Xu et al. ^[111] synthesized DF-Fe-N-C catalysts by the synergistic self-assembly of a silica and F127 based hard and soft-templates, respectively. Here, F127 acted as both structure-direct and pore construction agent (**Figure 9c**). The introduction of SiO₂ further enhanced porosity of material after acid-etching treatment, the fragmented carbon sheets were thin and defective in nature. Carbon nanotubes grafted in the 3D porous structure improved the electrical conductivity of the catalyst.

The results show that the prepared Fe-N/C-SA samples, benefiting from high accessibility of the active sites, showed excellent ORR activity with $E_{1/2}$ of 0.89 V in alkaline media compared to Pt/C (**Figure 10a**). The assembled zinc-air battery exhibited peak power density of 265.0 mW cm⁻² and large specific capacity of 798.2 mAh g⁻¹. The voltage gap of battery was not changed significantly after 70 h of cycling test, confirming the stability of the battery. From the results of the work of Shi et al. [110], the prepared catalyst (FeNC-DT) exhibited $E_{1/2}$ of 0.954 V under alkaline condition (**Figure 10b**). As reflected in polarization and power density curves in **Figure 10c**, zinc-air battery assembled using FeNC-DT outperformed precious metal catalysts in terms of power density. For the work of Xu et al. [111] (**Figure 10d**), the DT-Fe-N-C exhibited ORR with $E_{1/2}$ of 0.853 V and the zinc-air battery generated impressive powder density of 219 mW cm⁻².

3.2 Self-sacrificial templates

As discussed above, the template-assisted synthesis is a common method of designing hierarchically porous materials. However, it is difficult to control a size factor and stable template that is safe and simple to remove subsequently without disturbing the formed carbon framework. Therefore, the use of self-contained carbon species directly as templates to achieve tunable porous structured carbon materials is highly viable strategy. For this, biomass and small molecular building blocks including supramolecules and MOFs/COFs are the most suitable examples that not only produce required Fe₁-N_x-C materials but also convenient to tune their surface and interface properties by selection of precursor source materials. Metal center and dopant atoms of ligands in biomass, supramolecules and MOFs/COFs have multiple selectivity and can be used directly as templates.

3.2.1 MOFs/COFs

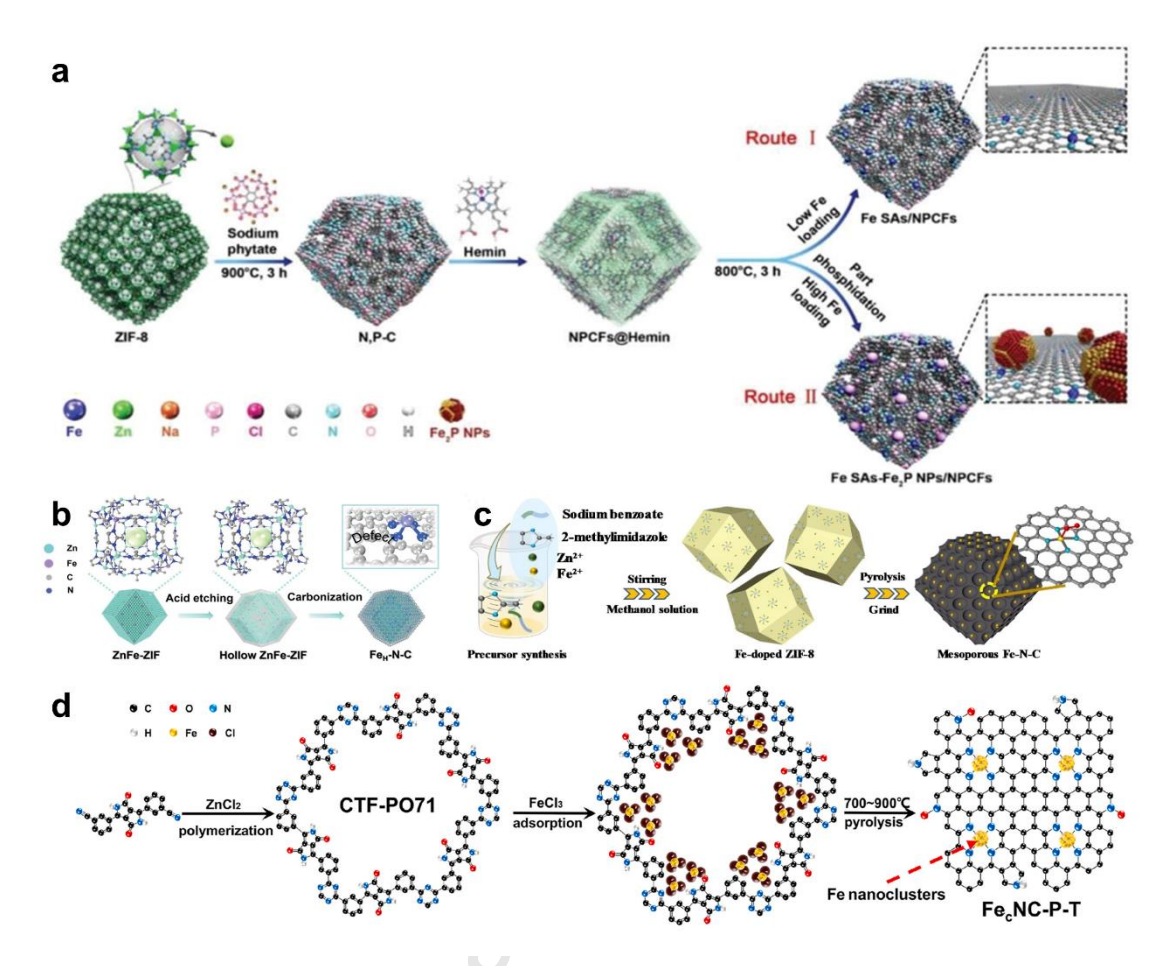


Figure 11. a) Schematic synthesis processes of Fe SAs/NPCFs and Fe SAs-Fe₂P NPs/NPCFs catalysts that uses ZIF-8 and sodium phytate mixture and pyrolyze at 900 °C to obtain NPCFs, and this product was further immersed in a low concentration of Hemin solution and pyrolyzed again to obtain the catalyst. [118] (Reproduced with permission. Copyrights (2022), John Wiley and Sons) b) Schematic illustration for design of Fe_H–N–C catalyst by utilizing ZnFe-ZIF with tannic acid etching agent. [119] (Reproduced with permission. Copyrights (2023), John Wiley and Sons) c) Schematic illustration for the synthesis of Fe-SA/Meso-C by pyrolysis of Fe-doped ZIF-8 followed by grinding and pyrolysis. [120] (Reproduced with permission. Copyrights (2022), Elsevier) d) Schematic illustration procedure for synthesis of Fe_cNC-P-T by utilizing CTF-PO71 COF that was impregnated with Fe³⁺ ions in the porous structure followed by pyrolysis. [40] (Reproduced with permission. Copyrights (2022), Elsevier)

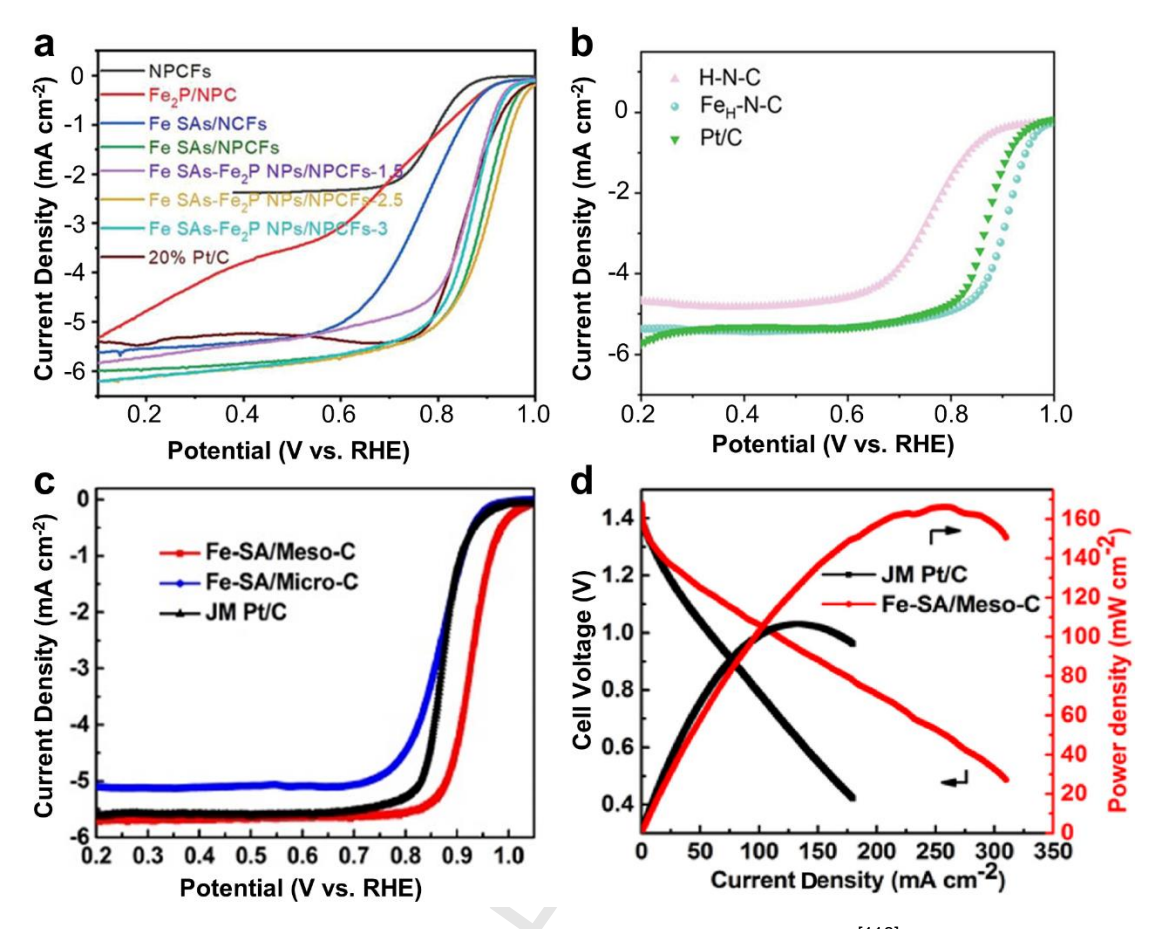


Figure 12. a) ORR LSV curves of Fe SAs/NCFs in 0.1 M KOH.^[118] (Reproduced with permission. Copyrights (2022), John Wiley and Sons) b) ORR LSV curves of Fe_H-N-C catalysts and Pt/C.^[119] (Reproduced with permission. Copyrights (2023), John Wiley and Sons) c) ORR LSV curves of Fe-SA/Micro-C, Fe-SA/Meso-C and JM Pt/C.^[120] (Reproduced with permission. Copyrights (2022), Elsevier) d) Discharge polarization and power density curves of Fe-SA/Meso-C and JM Pt/C based zinc-air batteries.^[120] (Reproduced with permission. Copyrights (2022), Elsevier)

MOF-based precursors provide unique backbone structure that can limit the metal migration and aggregation upon carbonization. [121–123] MOF-derived nanostructures offer (1) large surface area and this facilitates the exposure of more active sites; (2) tunable hierarchically porous structure that facilitates mass transfer reactions. [74] In addition, the strong interaction between the N- and metal atoms in MOF structure during pyrolysis could favor the formation of more intrinsic catalytically active sites. [124] In the work of Pan et al., [118] Fe SAs-Fe₂P NPs/NPCFs materials were prepared using in-situ doping—adsorption phosphide strategy with ZIF-8 (zeolitic-imidazolate framework, which is a type of MOFs family) as a template (**Figure 11a**). Moreover, catalysts with carbon vacancy defects have shown to enhance ORR catalysis. [125] Recently, in Tian et al. [119] work, carbon-vacancy modified Fe_H-N-C-SACs (Fe_H-N-C) material was synthesized using Zn-Fe-ZIF and tannic acid to form a hollow structure, following pyrolysis at 800 °C (**Figure 11b**). Here, tannic acid was used as hollow directing agent after etching. The mesoporous structure, well-known for increasing the effective contact area of reactants,

also accommodates changes in the carbon matrix during the electrochemical reactions and enhances the stability of the catalytic material. [126,127] Considering this, Wang et al. [120] developed sodium benzoate assisted self-templating strategy to synthesize Fe₁-N_x-C with mesoporous and microporous structures (Figure 11c). Weak interactions between the carboxylate anion of sodium benzoate and Fe ions were utilized to stabilize the Fe species in the carbon substrate. Furthermore, Gao and co-workers^[128] used ZIF-8 as self-template, and carbon and nitrogen source, to obtain Fe₁-N_x-C catalyst with a micro/mesoporous layered structure. The hydrogen concentration during pyrolysis was specified to effectively modulate the porous structure and active site density of the resulting carbon-based catalyst. Their study serves as a strong reference for the rational design of layered porous carbon-based materials and highly promising non-precious metal ORR catalysts. In addition to MOFs, COFs are emerging class of crystalline and porous polymers with high specific surface area and structural diversity, have also been considered as potential precursors for the preparation of high-performance M₁-N_x-Cbased electrocatalysts for ORR and zinc-air batteries. For example, Wang et al. [40] developed Fe-N_x nanoclusters containing porous carbon catalyst via pyrolyzing Fecontaining covalent-triazine organic frameworks (CTF-PO71) (Figure 11d).

These optimized Fe₁-N_x-C structures can deliver ORR catalytic performance with ultralow H₂O₂ product and stability in 10,000 cycles. [128] For example, the Fe SAs-Fe₂P NPs/NPCFs materials synthesized by Pan et al. [118] offered well balanced catalytic activity and stability due to the optimized structure comprising meso-micropores, and showed impressive ORR activity with high $E_{1/2}$ of 0.91 in alkaline electrolyte (**Figure 12a**). The results of the work of Tian et al.[119] revealed that Fe_H-N-C-SACs with unique hollow structure offered E_{1/2} of 0.91 V (**Figure 12b**), which is better than commercial Pt/C. In the work of Wang et al. [120], the as-synthesized Fe-N-C catalyst exhibited $E_{1/2}$ of 0.926 V in 0.1 M KOH (Figure 12c). The zinc-air battery assembled with this catalyst produced peak power density of 166.2 mW cm⁻² (**Figure 12d**). Likewise, Fe_{1.2}NC-0.02-800 deduced from CTF-PO71 COF with large specific surface area (1258 m² g⁻¹) and external surface area exhibited excellent ORR catalytic activity and zinc-air battery performance. [40] These results suggest that without the need for additional templates, complex activation and aggressive chemicals, the synthesized Fe₁-N_x-C can deliver high ORR catalytic activity and long-term durability in both three-electrode systems and assembled zinc-air batteries.

3.2.2 Biomass

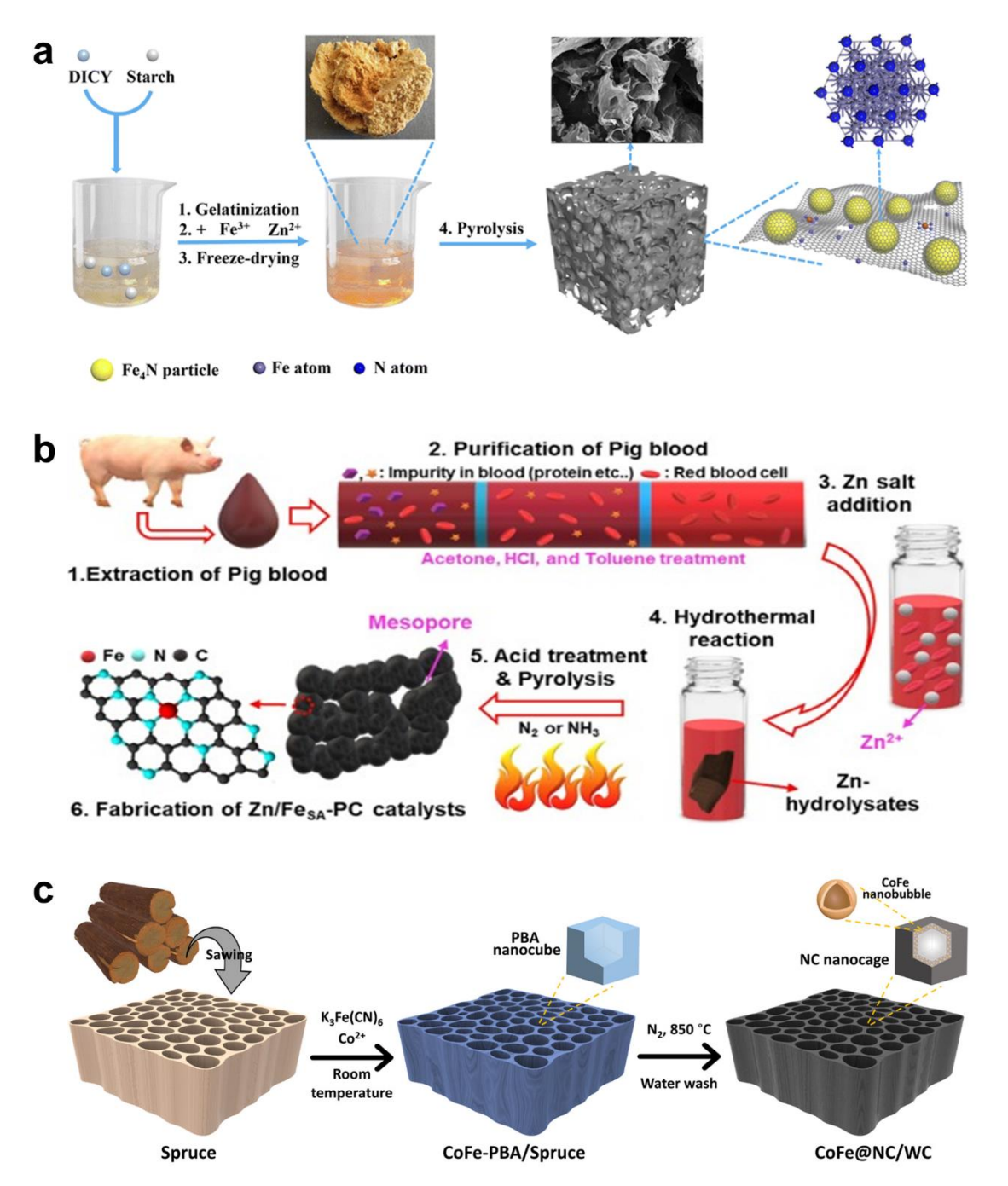


Figure 13. a) Schematic illustration for synthesis of Fe₄N@N-C by using Fe³⁺, Zn^{2+,} soluble starch and dicyandiamide mixture, first to obtain a hydrogel, and then the hydrogel was converted into an aerogel by freeze-drying, and pyrolyzed at 907 °C. [129] (Reproduced with permission. Copyrights (2023), Royal Society of Chemistry) b) Schematic preparation of Zn/FeSA-PC catalyst from waste pig blood, for this, zinc salt was added to the purified pig blood and Zn-hydrolysate was obtained via hydrothermal treatment and was pyrolyzed at 950 °C. [130] (Reproduced with permission. Copyrights (2021), Elsevier) c) Schematic illustration for the formation of CoFe@NC/WC from the wood infiltrated Fe³⁺ and Co²⁺ cations and then mixed with PBA followed by pyrolysis at 850 °C. [131] (Reproduced with permission. Copyrights (2023), John Wiley and Sons)

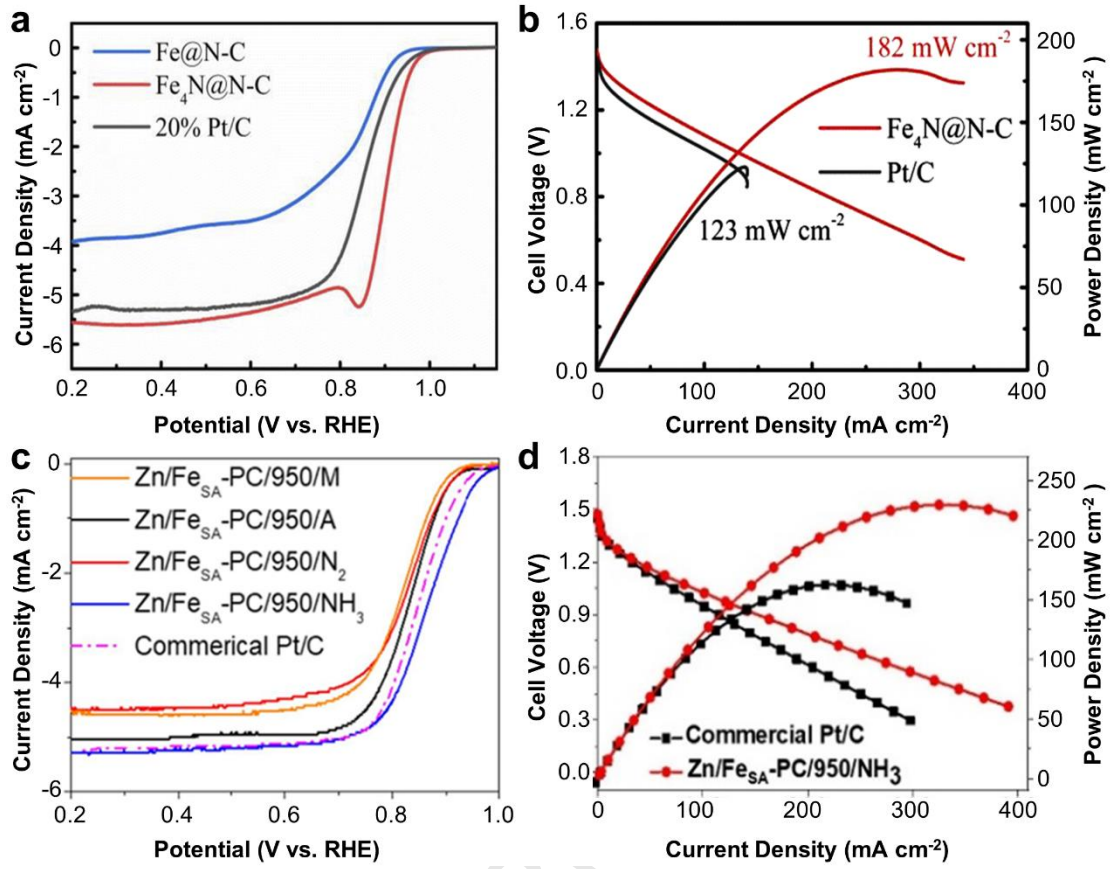


Figure 14. a) ORR LSV curves of Fe@N-C and Fe₄N@N-C in 0.1 M KOH. [129] (Reproduced with permission. Copyrights (2023), Royal Society of Chemistry) b) Discharge polarization and power density curves of zinc-air batteries with Fe₄N@N-C and Pt/C as cathodes. [129] (Reproduced with permission. Copyrights (2023), Royal Society of Chemistry) c) ORR LSV curves of Zn/Fe_{SA}-PC/950/NH₃ in O₂-saturated 0.1M KOH. [130] (Reproduced with permission. Copyrights (2021), Elsevier) d) Discharge polarization and power density curves of zinc-air batteries that used Zn/FeSA-PC/950/NH₃ and commercial Pt/C catalysts as cathode materials. [130] (Reproduced with permission. Copyrights (2021), Elsevier) All the LSV curves were collected at a rotation speed of 1600 rpm.

Biomass offers many advantages such as cost effectiveness, sustainability and ecofriendliness. Moreover, biomass can provide unique porous structure, which enhances electrolyte ion conductivity and contain large number of heteroatoms for efficient electrolyte accessibility and interaction. For these reasons, exploration of biomass-based carbon materials have also attracted considerable attention. As it was discussed earlier that Zn impregnated carbon based precursors produce porous carbon structures due to volatility of Zn at temperatures greater than 907 °C during the carbonization process. 133,134 The abundant oxygen in soluble starch can readily form complexation with Zn²+ ions. Based on these facts, Lu et al. 129 prepared porous structured Fe₄N@N-C materials by pyrolysis of starch with the assistance of zinc salt (**Figure 13a**). Animal blood is usually rich in Fe-porphyrins in hemoglobin and is therefore can be ideal precursor for the fabrication of Fe₁-N_x-C catalysts. 136–139 In the study of Kim et al., 130 the

waste pig blood was purified by solvents such as toluene and HCl and mixed with zinc source as sacrificial and activating template to synthesize Zn/FeSAPC/950/NH3 under reactive NH₃ atmosphere and resulted in highly dispersed Fe₁ sites and layered porous structures (Figure 13b). This strategy produced porous carbon with high specific surface area (1260 m² g-1) and layered porosity. Similarly, wood-based precursors can be interesting media.[140,141] As illustrated in Figure 13c, Ao et al.[131] prepared CoFe@NC/WC by using wood as a template and Prussian blue analogue (PBA, a kind of MOF-structure) was grown in-situ in the pores of wood and then pyrolyzed to obtain hierarchically porous structure. In the work of Lu et al., [129] the as-synthesized catalyst exhibited microporous, mesoporous and macro-porous hierarchically porous structure. The introduction of zinc in wood promoted the formation of porous structures and active sites, thus Fe₄N@N-C exhibited superior ORR activity with E_{1/2} of 0.903 V in alkaline media and zinc-air battery yielded peak power density of 182 mW cm⁻² (Figure 14a-b). Likewise, Zn/FeSAPC/950/NH₃ material^[130] also showed high E_{onset} and E_{1/2} values of 1.0 and 0.88 V, respectively (Figure 14c). Accordingly, their excellent performance was seen in zinc-air batteries with a maximum power density of 220 mW cm⁻² (Figure 14d). Asprepared CoFe@NC/WC catalyst showed ORR E_{1/2} of 0.8 V. [131]

3.2.3 Supramolecules

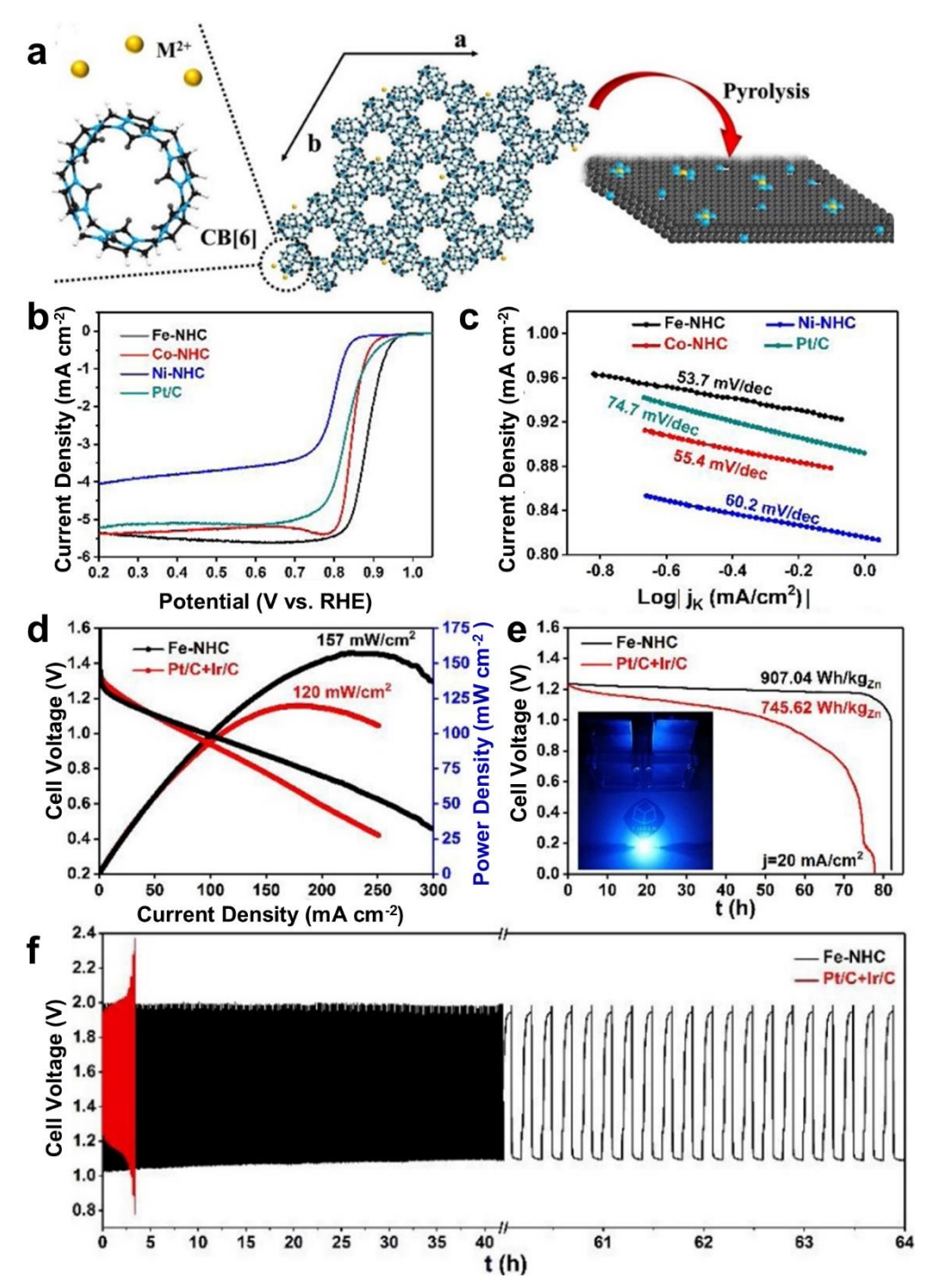


Figure 15. a) Schematic illustration for preparation of CB[6]-derived M-N-C single-atom catalysts. [142] (Reproduced with permission. Copyrights (2021), Elsevier) b) ORR LSV curves of CB[6]-derived M-N-C catalysts in O₂-saturated 0.1 M KOH solution at 1600 rpm. [142] (Reproduced with permission. Copyrights (2021), Elsevier) c) Tafel curves of CB [6]-derived M-N-C catalysts. [142] (Reproduced with permission. Copyrights (2021), Elsevier) d) Discharge polarization curves and corresponding power density curves of zinc-air batteries employing Fe-NHC and Pt/C+Ir/C catalysts for air electrodes. [142] (Reproduced with permission. Copyrights (2021), Elsevier) e) Discharge curves of zinc-air batteries at a discharging rate of 20 mA cm⁻². [142] (Reproduced with permission. Copyrights (2021), Elsevier) f) Discharge/charge cycling performance of Fe-NHC and

Pt/C+Ir/C based batteries at a current density of 10 mA cm⁻². [142] (Reproduced with permission. Copyrights (2021), Elsevier)

Supramolecules, which are covalently bonded organic units organized in an orderly fashion by weak intermolecular interactions, have been used to obtain porous carbon materials for a variety of applications, including electrochemical catalysis and zinc-air batteries. For instance, a series of M-N-C (M = Fe, Co and Ni) monatomic electrocatalysts were synthesized using macrocyclic cucurbit uril CB[6] self-assembly as a precursor by Zhang et al. [142] As displayed in **Figure 15a**, this self-template method using macrocyclic CB[6] self-assembly yielded hierarchical micro/mesoporous structure. By pyrolysis of mixture of Fe (or Co, Ni) chlorides and CB[6], the catalysts possess pores spread throughout the carbon matrix. Therefore, Fe-NHC exhibited high ORR activity with E_{onset} of 0.94 V and E_{1/2} of 0.89 V (**Figure 15b**), as well as a low Tafel slope of 53.7 mV dec⁻¹ (**Figure 15c**). The zinc-air battery offered a peak power density of 157 mW cm⁻² (**Figure 15d**) while generating high energy density of 907.04 Wh kg_{Zn}⁻¹ (**Figure 15e**). At the same time, the battery showed a good charge/discharge cycle stability with no significant degradation in the voltage gap during 60 h operation (**Figure 15f**).

Table 1. Structural parameters and electrochemical performance metrics of representative Fe_1-N_x-C based catalysts in ORR and zinc-air batteries in alkaline condition (0.1 M KOH).

Catalysts	Strategies	Specific	E _{1/2} (V vs.	Peak power	Refs
	(templates)	surface area	RHE)	density (mW cm ⁻	
		(m ² g ⁻¹)		²)	
Fe-N-MCNs	Soft-template	596	0.830		78
MF-C-Fe-Phen-800	Soft-template	807	0.871	235	80
FePNC	Soft-template	300	0.900	98	81
FeCo-NSC	Soft-template		0.860	153	82
Fe/N/C	Hard-template		0.900	181	93
Fe-N-HMC	Hard-template	733	0.856		91
Fe/RNC	Hard-template	793	0.912	159	92
Fe-N-C	Hard melt	1061	0.895	175	97
HPFe-N-C	Hard melt	1605	0.911	160	96
Fe-N-C-900	Hard melt	837	0.927		95
Fe-N/C-SA	Hard and soft- template	658	0.890	265	109
FeNC-DT	Hard and soft- template	999	0.954	178	110
DT-Fe-N-C	Hard and soft- template	990	0.853	219	112
Fe SAs-Fe₂P NPs/NPCFs	MOF	1009	0.910		118
Fe _H -N-C	MOF	1071	0.910	225	119
Fe-SA/Meso-C	MOF	884	0.926	166	120
Fe₄N@N-C	Biomass	378	0.903	182	129
Zn/FeSA- PC/950/NH₃	Biomass	1260	0.880	220	130
CoFe@NC/WC	Biomass		0.800	139	131
Fe-NHC	Supermolecules	729	0.890	157	142

4. Summary and perspective

The design of hierarchical porous nanostructures plays an important role in enhancing the ORR performance, especially for electron transport and mass transfer characteristics in the zinc-air batteries. We discussed the details of structural design and application of hierarchical porous Fe₁-Nx-C based ORR catalysts for zinc-air batteries. For example, in the template methods, although, it is easy to adjust the pore size by selecting the template parameters, there still exists the following problems: (1) The hard-templates mostly generate mesoporous and/or macroporous carbon substrate with relatively low specific surface area. High stability of the hard-templates makes their post-carbonization removal challenging and often requires the use of strong acids/bases, which not only increases the cost and safety issue of the process, but also it is not conducive to the commercial development of large-scale production. (2) The soft-templates are limited by their relatively low thermal stability therefore it often poses changes in obtaining targeted porosity with well-defined porous structure. Soft-templates are relatively expensive to produce large scale porous carbon materials. (3) The relatively low template content of biomass materials can limit their effectiveness of producing hollow and/or hierarchical porous structured carbon materials. (4) MOFs/COFs and supramolecular-derived materials, which have been widely studied, are complex and expensive to synthesize, and the collapse of the structure and volatility of ligands during the pyrolysis process can lead to metal particle aggregation along with the production of low porosity carbon materials in the low yields which is a limiting factor for their full application potential. In summary, the combination of hard- and soft-template and/or self-template method can offer attractive prospects in generating hierarchical porous carbon structures with finely distributed and highly accessible M₁-N_x active sites in the heterogeneous surface and balance binding energies to promote the catalysis reactions efficiently. Clearly, carbon support characteristic porosity, such as specific surface area, pore-sizes, pose-size distribution and pore volume play key role in promoting their intrinsic electrocatalytic activity. Here, it is worth noting that MOFs as self-sacrificial templates to generate such functional catalysts can be reminiscent to the structures derived from the combined hardand soft-templates. Moreover, the catalysts with high porosity or specific surface area appear to offer high ORR activity and enable relevant zinc-air battery performance efficiently.

As discussed, the hierarchical porous structured carbon supports have shown to perform efficiently for both ORR and zinc-air battery. For example, as summarized in **Table 1**, the hierarchical porous Fe_1 - N_x -C catalysts with relatively high specific surface area have offered excellent ORR performance with $E_{1/2}$ values exceeding 0.9 V (vs. RHE) and delivered high discharge peak power density values in zinc-air battery. As it can be seen, such structure-relevant performances are linked to the development of catalyst materials from the combination of hard- and soft-template synthesis route. Further best catalytic performance for ORR and zinc-air battery can be observed from MOFs-derived Fe_1 - N_x -C catalysts as they also appear to offer high specific surface area hierarchical porous structures. Such high activities of the catalyst materials have been also linked to relative concentrations of pyridinic-N and graphitic-N along with specific Fe- N_x coordination as

they can promote the Fe-coordination, O2 adsorption and ORR via electron-accepting $nature.^{[80,95,96,109,110,118,120,129,131,142]} \ \ Moreover, \ the \ defective \ carbon \ sites \ and \ electron$ donating P-dopants have been identified to enhance the ORR.[81,118,119] Accordingly, such high performing functional M₁-N_x-C catalysts can be readily generated by utilizing bimetallic MOFs comprising combination of volatile and graphitizable metal centers of Zn and Fe (or Co or Ni), respectively. Here, oxidation, reduction and evaporation of Zn centers (e.g. via 2Zn + $O_2 \rightarrow ZnO$; 2ZnO + C \rightarrow 2Zn + CO_2 + C) can generate highly hierarchical porous carbon as mesoporosity associated with ZnO impregnation (i.e. porogen) followed by its reduction and evaporation contribute to microporosity, where, Fe-related metallic centers can act as graphitization agents for the MOF ligand to generate desirable electrically conducting graphitic component.[144-146] Likewise, highly flexible, tunable surface functionality and electrochemically benign porous graphenenetworks, conducting carbon black and graphitic carbon nanotubes (e.g. porous Ketjenblack, usual electrode additive as conducting agent)-based materials hybridized with MOFs-related precursors can also readily generate highly efficient bifunctional M₁-N_x-C catalysts with high performance in zinc-air battery. [147-150]

Declaration of competing interest

The authors declare that they have no known competing financial interests or personal relationships that could have appeared to influence the work reported in this paper.

Acknowledgements

This work was supported by the China Postdoctoral Science Foundation (2021M702323), the Sichuan University Postdoctoral Interdisciplinary Innovation Fund (JCXK2213), the Special fund for postdoctoral research project from Sichuan Province, the Science Specialty Program of Sichuan University (Grant. No. 2020SCUNL210), and The Royal Academy of Engineering for the financial support of Brett (RCSRF2021/13/53) under the Research Chairs and Senior Research Fellowships scheme.

References

- [1] Y. Li, H. Dai, Chem. Soc. Rev. 2014, 43, 5257.
- [2] H. Liu, W. Xie, Z. Huang, C. Yao, Y. Han, W. Huang, *Small Methods* **2022**, *6*, 2101116.
- [3] X. Zou, M. Tang, Q. Lu, Y. Wang, Z. Shao, L. An, *Energy Environ. Sci.* **2024**, 17, 386.
- [4] F. Abdelghafar, X. Xu, S. P. Jiang, Z. Shao, *Mater. Rep. Energy* **2022**, 2, 100144.
- [5] Z. Meng, N. Chen, S. Cai, R. Wang, J. Wu, H. Tang, *Mater. Chem. Front.* **2021**, 5, 2649.
- [6] I. S. Amiinu, X. Liu, Z. Pu, W. Li, Q. Li, J. Zhang, H. Tang, H. Zhang, S. Mu, Adv. Funct. Mater. 2018, 28, 1704638.
- [7] S. Cai, R. Wang, W. Guo, H. Tang, *Langmuir* **2018**, *34*, 1992.
- [8] Y. Wang, Q. Cao, C. Guan, C. Cheng, Small 2020, 16, 2002902.

- [9] S. Zhao, H. Yin, L. Du, L. He, K. Zhao, L. Chang, G. Yin, H. Zhao, S. Liu, Z. Tang, *ACS Nano* **2014**, *8*, 12660.
- [10] J. Yin, Y. Li, F. Lv, Q. Fan, Y.-Q. Zhao, Q. Zhang, W. Wang, F. Cheng, P. Xi, S. Guo, ACS Nano 2017, 11, 2275.
- [11] D. Wang, P. Yang, H. Xu, J. Ma, L. Du, G. Zhang, R. Li, Z. Jiang, Y. Li, J. Zhang, M. An, J. Power Sour. 2021, 485, 229339.
- [12] N. Logeshwaran, S. Ramakrishnan, S. S. Chandrasekaran, M. Vinothkannan, A. R. Kim, S. Sengodan, D. B. Velusamy, P. Varadhan, J.-H. He, D. J. Yoo, *Appl. Catal. B: Environ.* 2021, 297, 120405.
- [13] J. Wang, J. Xu, X. Guo, T. Shen, C. Xuan, B. Tian, Z. Wen, Y. Zhu, D. Wang, *Appl. Catal. B: Environ.* **2021**, 298, 120539.
- [14] Z. Guan, X. Zhang, J. Fang, X. Wang, W. Zhu, Z. Zhuang, *Mater. Lett.* 2020, 258, 126826.
- [15] L. Song, T. Wang, L. Li, C. Wu, J. He, Appl. Catal. B: Environ. 2019, 244, 197.
- [16] K. Im, D. Kim, J.-H. Jang, J. Kim, S. J. Yoo, Appl. Catal. B: Environ. 2020, 260, 118192.
- [17] G.-S. Kang, G. Lee, S. Y. Cho, H.-I. Joh, D. C. Lee, S. Lee, *Appl. Surf. Sci.* **2021**, *548*, 149027.
- [18] H.-F. Wang, C. Tang, Q. Zhang, Adv. Funct. Mater. 2018, 28, 1803329.
- [19] Q. Qin, H. Jang, P. Li, B. Yuan, X. Liu, J. Cho, *Adv. Energy Mater.* **2019**, *9*, 1803312.
- [20] L. Liu, G. Zeng, J. Chen, L. Bi, L. Dai, Z. Wen, *Nano Energy* **2018**, *49*, 393.
- [21] Q. Wang, Y. Ji, Y. Lei, Y. Wang, Y. Wang, Y. Li, S. Wang, *ACS Energy Lett.* **2018**, *3*, 1183.
- [22] N. Li, L. Li, J. Xia, M. Arif, S. Zhou, G. He, H. Chen, *J. Mater. Sci. Techn.* **2023**, *139*, 224.
- [23] X. Wang, X. Fan, H. Lin, H. Fu, T. Wang, J. Zheng, X. Li, *RSC Adv.* **2016**, *6*, 37965.
- [24] L. Li, Y.-J. Chen, H.-R. Xing, N. Li, J.-W. Xia, X.-Y. Qian, H. Xu, W.-Z. Li, F.-X. Yin, G.-Y. He, H.-Q. Chen, *Nano Res.* **2022**, *15*, 8056
- [25] L. Peng, J. Yang, Y. Yang, F. Qian, Q. Wang, D. Sun-Waterhouse, L. Shang, T. Zhang, G. I. N. Waterhouse, *Ad. Mater.* **2022**, *34*, 2202544.
- [26] Y. He, Q. Tan, L. Lu, J. Sokolowski, G. Wu, *Electrochem. Energy Rev.* **2019**, 2, 231.
- [27] H. Fei, J. Dong, C. Wan, Z. Zhao, X. Xu, Z. Lin, Y. Wang, H. Liu, K. Zang, J. Luo, S. Zhao, W. Hu, W. Yan, I. Shakir, Y. Huang, X. Duan, *Adv. Mater.* 2018, 30, 1802146.
- [28] J.-J. Cai, Q.-Y. Zhou, B. Liu, X.-F. Gong, Y.-L. Zhang, K. Goh, D.-M. Gu, L. Zhao, X.-L. Sui, Z.-B. Wang, *Nanoscale* **2020**, *12*, 973.
- [29] H. Li, C. Xu, W. Wang, G. Li, J. Huang, L. Chen, Z. Hou, *J. Electroanalytical Chem.* **2023**, *935*, 117316.
- [30] X. Xu, C. Shu, R. Jin, H. Chen, C. Xu, Y. Liu, L. Sun, C. Guo, H. Chen, W. Liao, *Electrochim. Acta* **2023**, *465*, 142986.
- [31] A. Zhou, D. Wang, Y. Li, *Microstructures* **2022**, *2*, 2022005.

- [32] S. Gao, B. Fan, R. Feng, C. Ye, X. Wei, J. Liu, X. Bu, *Nano Energy* **2017**, *40*, 462.
- [33] H. Li, Z. Zhang, M. Dou, F. Wang, Chem. Eur. J. 2018, 24, 8848.
- [34] Y. Yuan, Y. Liu, C. Li, S. Feng, Q. Liu, J. Huo, J. Alloys Comp. 2022, 920, 165821.
- [35] U. Martinez, S. Komini Babu, E. F. Holby, H. T. Chung, X. Yin, P. Zelenay, *Adv. Mater.* **2019**, *31*, 1806545.
- [36] M. Lefèvre, E. Proietti, F. Jaouen, J.-P. Dodelet, Science 2009, 324, 71.
- [37] X. Lyu, G. Li, X. Chen, B. Shi, J. Liu, L. Zhuang, Y. Jia, *Small Methods* **2019**, *3*, 1800450.
- [38] B. Qiao, A. Wang, X. Yang, L. F. Allard, Z. Jiang, Y. Cui, J. Liu, J. Li, T. Zhang, *Nat. Chem.* **2011**, *3*, 634.
- [39] G. Zhang, Y. Jia, C. Zhang, X. Xiong, K. Sun, R. Chen, W. Chen, Y. Kuang, L. Zheng, H. Tang, W. Liu, X. Sun, W. Lin, H. Dai, *Energy Environ. Sci.*, **2019**, *12*, 1317.
- [40] Z. Wang, L. Zhou, R. Li, K. Qu, L. Wang, W. Kang, H. Li, S. Xiong, *Microp. Mesop. Mater.* 2022, 330, 111609.
- [41] H. Yan, H. Cheng, H. Yi, Y. Lin, T. Yao, C. Wang, J. Li, S. Wei, J. Lu, *J. Am. Chem. Soc.* **2015**, *137*, 10484.
- [42] H. Wei, X. Liu, A. Wang, L. Zhang, B. Qiao, X. Yang, Y. Huang, S. Miao, J. Liu, T. Zhang, *Nat. Commun.* **2014**, *5*, 5634.
- [43] P. Hu, Z. Huang, Z. Amghouz, M. Makkee, F. Xu, F. Kapteijn, A. Dikhtiarenko, Y. Chen, X. Gu, X. Tang, *Angew. Chem. Int. Ed.* **2014**, *53*, 3418.
- [44] L. Fan, P. F. Liu, X. Yan, L. Gu, Z. Z. Yang, H. G. Yang, S. Qiu, X. Yao, *Nat. Commun.* **2016**, *7*, 10667.
- [45] D. Liu, X. Li, S. Chen, H. Yan, C. Wang, C. Wu, Y. A. Haleem, S. Duan, J. Lu,
 B. Ge, P. M. Ajayan, Y. Luo, J. Jiang, L. Song, *Nat. Energy* 2019, 4, 512.
- [46] Z. Li, R. Gao, M. Feng, Y. Deng, D. Xiao, Y. Zheng, Z. Zhao, D. Luo, Y. Liu, Z. Zhang, D. Wang, Q. Li, H. Li, X. Wang, Z. Chen, *Adv. Energy Mater.* 2021, 11, 2003291.
- [47] A. Zitolo, V. Goellner, V. Armel, M.-T. Sougrati, T. Mineva, L. Stievano, E. Fonda, F. Jaouen, *Nat. Mater.* **2015**, *14*, 937.
- [48] F. Pan, B. Li, E. Sarnello, Y. Fei, X. Feng, Y. Gang, X. Xiang, L. Fang, T. Li, Y. H. Hu, G. Wang, Y. Li, *ACS Catal.* **2020**, *10*, 10803.
- [49] F.-L. Meng, Z.-L. Wang, H.-X. Zhong, J. Wang, J.-M. Yan, X.-B. Zhang, *Adv. Mater.* **2016**, *28*, 7948.
- [50] Q. Liu, Z. Chang, Z. Li, X. Zhang, Small Methods **2018**, 2, 1700231.
- [51] Q. Wei, Y. Fu, G. Zhang, S. Sun, Current Opinion Electrochem. 2017, 4, 45.
- [52] N. Xu, J. Qiao, Q. Nie, M. Wang, H. Xu, Y. Wang, X.-D. Zhou, *Catal. Today* **2018**, *318*, 144.
- [53] L. Yang, X. Zeng, D. Wang, D. Cao, Energy Storage Mater. 2018, 12, 277.
- [54] J. Chen, C. Fan, X. Hu, C. Wang, Z. Huang, G. Fu, J.-M. Lee, Y. Tang, *Small* **2019**, *15*, 1901518.
- [55] J. Pan, Y. Y. Xu, H. Yang, Z. Dong, H. Liu, B. Y. Xia, Adv. Sci. 2018, 5,

- 1700691.
- [56] H. Li, L. Ma, C. Han, Z. Wang, Z. Liu, Z. Tang, C. Zhi, *Nano Energy* 2019, 62, 550.
- [57] J. Fu, D. U. Lee, F. M. Hassan, L. Yang, Z. Bai, M. G. Park, Z. Chen, *Adv. Mater.* **2015**, *27*, 5617.
- [58] C. Zhu, Y. Ma, W. Zang, C. Guan, X. Liu, S. J. Pennycook, J. Wang, W. Huang, *Chem. Eng. J.* **2019**, *369*, 988.
- [59] Y. Zhang, H. Sun, Y. Qiu, X. Ji, T. Ma, F. Gao, Z. Ma, B. Zhang, P. Hu, *Carbon* **2019**, *144*, 370.
- [60] Y. Zhong, Z. Pan, X. Wang, J. Yang, Y. Qiu, S. Xu, Y. Lu, Q. Huang, W. Li, Adv. Sci. 2019, 6, 1802243.
- [61] D. U. Lee, J. Choi, K. Feng, H. W. Park, Z. Chen, Adv. Energy Mater. 2014, 4, 1301389
- [62] D. Yang, L. Zhang, X. Yan, X. Yao, Small Methods 2017, 1, 1700209.
- [63] M. Zihan, C. Shichang, T. Wenmao, T. Haolin, *J. Nanosci. Nanotech.* **2020**, 2. 1085.
- [64] W. Lei, Y.-P. Deng, G. Li, Z. P. Cano, X. Wang, D. Luo, Y. Liu, D. Wang, Z. Chen, ACS Catal. 2018, 8, 2464.
- [65] J. Wu, H. Zhou, Q. Li, M. Chen, J. Wan, N. Zhang, L. Xiong, S. Li, B. Y. Xia, G. Feng, M. Liu, L. Huang, Adv. Energy Mater. 2019, 9, 1900149.
- [66] Z. Wang, H. Jin, T. Meng, K. Liao, W. Meng, J. Yang, D. He, Y. Xiong, S. Mu, Adv. Funct. Mater. 2018, 28, 1802596.
- [67] G. Fu, Y. Tang, J. Lee, ChemElectroChem 2018, 5, 1424.
- [68] Y. Han, Y.-G. Wang, W. Chen, R. Xu, L. Zheng, J. Zhang, J. Luo, R.-A. Shen, Y. Zhu, W.-C. Cheong, C. Chen, Q. Peng, D. Wang, Y. Li, J. Am. Chem. Soc. 2017, 139, 17269.
- [69] H. Zeng, W. Wang, J. Li, J. Luo, S. Chen, ACS Appl. Mater. Interf. 2018, 10, 8721.
- [70] D. Luo, B. Chen, X. Li, Z. Liu, X. Liu, X. Liu, C. Shi, X. S. Zhao, J. Mater. Chem. A 2018, 6, 7897.
- [71] J. Wei, Y. Liang, X. Zhang, G. P. Simon, D. Zhao, J. Zhang, S. Jiang, H. Wang, *Nanoscale* **2015**, 7, 6247.
- [72] T. Sun, L. Xu, S. Li, W. Chai, Y. Huang, Y. Yan, J. Chen, *Appl. Catal. B: Environ.* **2016**, *193*, 1.
- [73] Z. Liang, C. Zhang, H. Yuan, W. Zhang, H. Zheng, R. Cao, *Chem. Commun.* **2018**, *54*, 7519.
- [74] W. Zhang, R. Cheng, H. Bi, Y. Lu, L. Ma, X. He, *New Carbon Mater.* **2021**, *36*, 69.
- [75] K. Li, J. Yang, R. Huang, S. Lin, J. Gu, Angew. Chem. Int. Ed. 2020, 59, 14124.
- [76] T. Zhao, A. Elzatahry, X. Li, D. Zhao, Nat. Rev. Mater. 2019, 4, 775.
- [77] B. Hu, Y. Zhao, H.-Z. Zhu, S.-H. Yu, ACS Nano 2011, 5, 3166.
- [78] J. Wei, Y. Liang, X. Zhang, G. P. Simon, D. Zhao, J. Zhang, S. Jiang, H. Wang, *Nanoscale* **2015**, *7*, 6247.
- [79] R. Xing, T. Zhou, Y. Zhou, R. Ma, Q. Liu, J. Luo, J. Wang, Nano-Micro Lett.

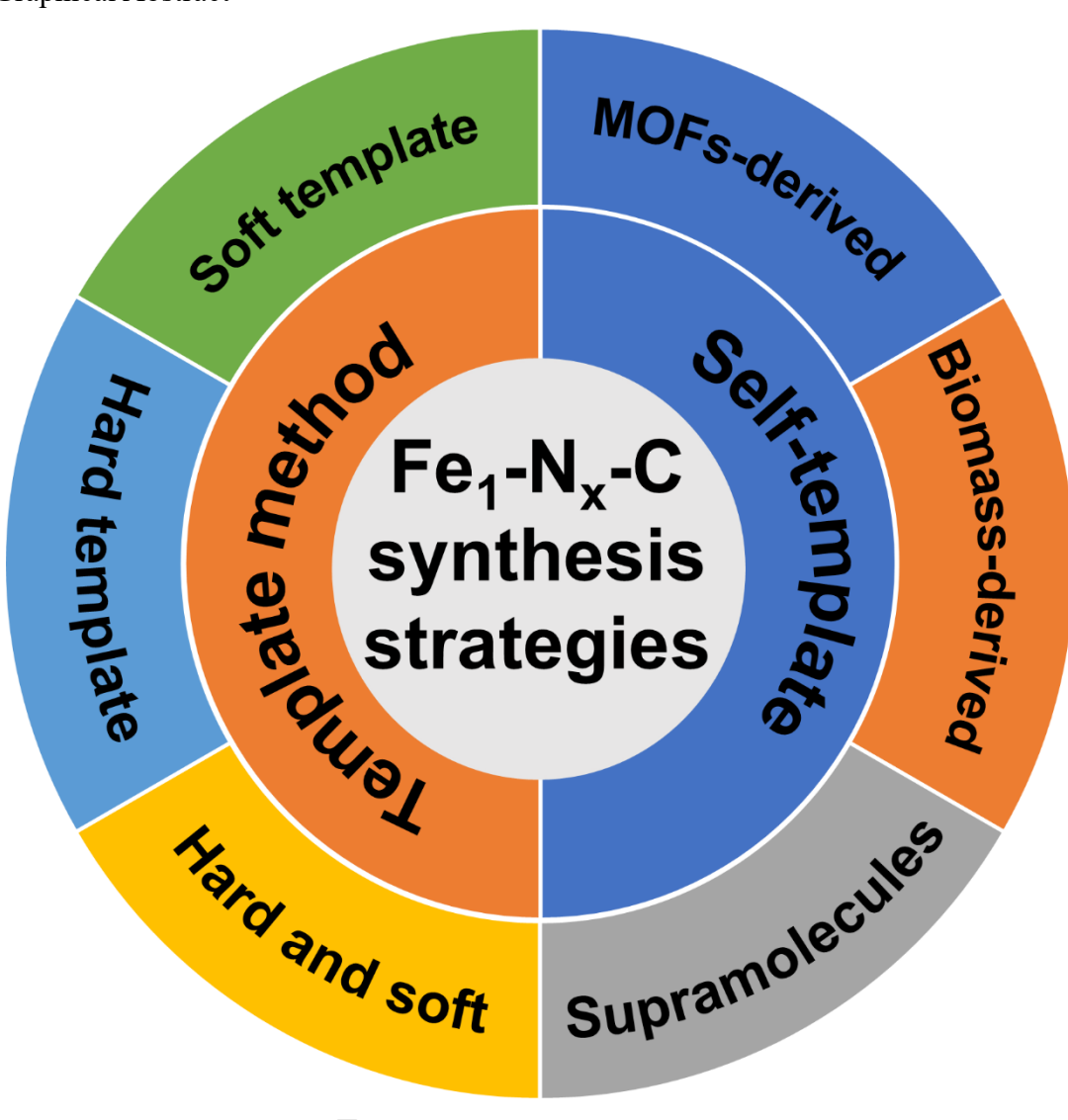
- **2017**, 10, 3.
- [80] M. Hao, R. Dun, Y. Su, W. Li, Nanoscale 2020, 12, 15115.
- [81] H. Liu, L. Jiang, Y. Sun, J. Khan, B. Feng, J. Xiao, H. Zhang, H. Xie, L. Li, S. Wang, L. Han, *Adv. Energy Mater.* **2023**, *13*, 2301223.
- [82] Y. Wu, C. Ye, L. Yu, Y. Liu, J. Huang, J. Bi, L. Xue, J. Sun, J. Yang, W. Zhang, X. Wang, P. Xiong, J. Zhu, *Energy Storage Mater.* **2022**, *45*, 805.
- [83] X. Han, X. Ling, D. Yu, D. Xie, L. Li, S. Peng, C. Zhong, N. Zhao, Y. Deng, W. Hu, Adv. Mater. 2019, 31, 1905622.
- [84] G. Yang, J. Zhu, P. Yuan, Y. Hu, G. Qu, B.-A. Lu, X. Xue, H. Yin, W. Cheng, J. Cheng, W. Xu, J. Li, J. Hu, S. Mu, J.-N. Zhang, *Nat. Commun.* 2021, 12, 1734.
- [85] J. Zhang, Q. Huang, J. Wang, J. Zhang, Y. Zhao, *Chinese J. Catal.* **2020**, *41*, 783.
- [86] Y. Jia, F. Zhang, Q. Liu, J. Yang, J. Xian, Y. Sun, Y. Li, G. Li, *Chinese Chem. Lett.* **2022**, *33*, 1070.
- [87] Q. Xu, J. Zhang, D. Wang, Y. Li, Chinese Chem. Lett. 2021, 32, 3771.
- [88] H. Shang, X. Zhou, J. Dong, A. Li, X. Zhao, Q. Liu, Y. Lin, J. Pei, Z. Li, Z. Jiang, D. Zhou, L. Zheng, Y. Wang, J. Zhou, Z. Yang, R. Cao, R. Sarangi, T. Sun, X. Yang, X. Zheng, W. Yan, Z. Zhuang, J. Li, W. Chen, D. Wang, J. Zhang, Y. Li, *Nat. Commun.* 2020, 11, 3049.
- [89] S. Schacht, Q. Huo, I. G. Voigt-Martin, G. D. Stucky, F. Schüth, *Science* **1996**, 273, 768.
- [90] H. M. Duan, S. Q. Liu, Appl. Mechanics Mater. 2014, 670–671, 279.
- [91] T. Zhu, W. Lyu, Y. Wang, X. Mi, Y. Liao, J. Colloid Interface Sci. 2023, 633, 265.
- [92] R. Zhao, H. Wang, X. Zhang, J. Liu, G. Du, T. Chen, *Langmuir* **2022**, *38*, 11372.
- [93] L. Wu, B. Ni, R. Chen, P. Sun, T. Chen, J. Mater. Chem. A 2020, 8, 21026.
- [94] D. Wang, H. Xu, P. Yang, L. Xiao, L. Du, X. Lu, R. Li, J. Zhang, M. An, J. Mater. Chem. A 2021, 9, 9761.
- [95] C. Zhu, Q. Shi, B. Z. Xu, S. Fu, G. Wan, C. Yang, S. Yao, J. Song, H. Zhou, D. Du, S. P. Beckman, D. Su, Y. Lin, Adv. Energy Mater. 2018, 8, 1801956.
- [96] H. Xu, D. Wang, P. Yang, L. Du, X. Lu, R. Li, L. Liu, J. Zhang, M. An, Appl. Catal. B: Environ. 2022, 305, 121040.
- [97] X. Lu, H. Xu, P. Yang, L. Xiao, Y. Li, J. Ma, R. Li, L. Liu, A. Liu, V. Kondratiev, O. Levin, J. Zhang, M. An, Appl. Catal. B: Environ. 2022, 313, 121454.
- [98] D. Inman, S. H. White, J. Appl. Electrochem. 1978, 8, 375.
- [99] G. Z. Chen, D. J. Fray, T. W. Farthing, *Nature* **2000**, *407*, 361.
- [100] T. Nohira, K. Yasuda, Y. Ito, Nat. Mater. 2003, 2, 397.
- [101] D. E. Bugaris, H.-C. zur Loye, *Angew. Chemie Int. Ed.* **2012**, *51*, 3780.
- [102] J. Hu, D. Wu, C. Zhu, C. Hao, C. Xin, J. Zhang, J. Guo, N. Li, G. Zhang, Y. Shi, *Nano Energy* **2020**, 72, 104670.
- [103] Y. Chen, S. Ji, Y. Wang, J. Dong, W. Chen, Z. Li, R. Shen, L. Zheng, Z.

- Zhuang, D. Wang, Y. Li, Angew. Chemie Int. Ed. 2017, 56, 6937.
- [104] C. Zhu, S. Fu, J. Song, Q. Shi, D. Su, M. H. Engelhard, X. Li, D. Xiao, D. Li, L. Estevez, D. Du, Y. Lin, *Small* **2017**, *13*, 1603407.
- [105] H. Shen, E. Gracia-Espino, J. Ma, K. Zang, J. Luo, L. Wang, S. Gao, X. Mamat, G. Hu, T. Wagberg, S. Guo, *Angew. Chemie Int. Ed.* **2017**, *56*, 13800.
- [106] P. Yin, T. Yao, Y. Wu, L. Zheng, Y. Lin, W. Liu, H. Ju, J. Zhu, X. Hong, Z. Deng, G. Zhou, S. Wei, Y. Li, Angew. Chemie Int. Ed. 2016, 55, 10800.
- [107] J. Hu, D. Wu, C. Zhu, C. Hao, C. Xin, J. Zhang, J. Guo, N. Li, G. Zhang, Y. Shi, Nano Energy 2020, 72, 104670.
- [108] Z. Mao, M. Wang, L. Liu, L. Peng, S. Chen, L. Li, J. Li, Z. Wei, *Chinese J. Catal.* **2020**, *41*, 799.
- [109] Y. Song, W. Li, Y. Ma, S. Tang, H. Wang, Q. Wang, J. Power Sour. 2022, 545, 231913.
- [110] J. Shi, H. Shao, F. Yang, J. Li, L. Fan, W. Cai, *Chem. Eng. J.* **2022**, *445*, 136628.
- [111] X. Xu, C. Xu, J. Liu, R. Jin, X. Luo, C. Shu, H. Chen, C. Guo, L. Xu, Y. Si, *J. Alloys Comp.* **2023**, *939*, 168782.
- [112] H. Wang, J. Li, K. Li, Y. Lin, J. Chen, L. Gao, V. Nicolosi, X. Xiao, J.-M. Lee, *Chem. Soc. Rev.* **2021**, *50*, 1354.
- [113] F. Dong, M. Wu, Z. Chen, X. Liu, G. Zhang, J. Qiao, S. Sun, *Nano-Micro Lett.* **2022**, *14*, 36.
- [114] J. Liang, R. F. Zhou, X. M. Chen, Y. H. Tang, S. Z. Qiao, *Adv. Mater.* **2014**, *26*, 6074.
- [115] Z. Zhu, H. Yin, Y. Wang, C. Chuang, L. Xing, M. Dong, Y. Lu, G. Casillas-Garcia, Y. Zheng, S. Chen, Y. Dou, P. Liu, Q. Cheng, H. Zhao, *Adv. Mater.* 2020, 32, 2004670.
- [116] I. Kone, A. Xie, Y. Tang, Y. Chen, J. Liu, Y. Chen, Y. Sun, X. Yang, P. Wan, *ACS Appl. Mater. Interfaces* **2017**, *9*, 20963.
- [117] P. Zhang, L. Wang, S. Yang, J. A. Schott, X. Liu, S. M. Mahurin, C. Huang, Y. Zhang, P. F. Fulvio, M. F. Chisholm, S. Dai, *Nat. Commun.* **2017**, *8*, 15020.
- [118] Y. Pan, X. Ma, M. Wang, X. Yang, S. Liu, H. Chen, Z. Zhuang, Y. Zhang, W. Cheong, C. Zhang, X. Cao, R. Shen, Q. Xu, W. Zhu, Y. Liu, X. Wang, X. Zhang, W. Yan, J. Li, H. M. Chen, C. Chen, Y. Li, Ad. Mater. 2022, 34, 2203621.
- [119] H. Tian, A. Song, P. Zhang, K. Sun, J. Wang, B. Sun, Q. Fan, G. Shao, C. Chen, H. Liu, Y. Li, G. Wang, Adv. Mater. 2023, 35, 2210714.
- [120] X. Wang, H. Zhu, C. Yang, J. Lu, L. Zheng, H.-P. Liang, *Carbon* **2022**, *191*, 393.
- [121] Q. Lai, L. Zheng, Y. Liang, J. He, J. Zhao, J. Chen, ACS Catal. 2017, 7, 1655.
- [122] J. Wang, G. Han, L. Wang, L. Du, G. Chen, Y. Gao, Y. Ma, C. Du, X. Cheng, P. Zuo, G. Yin, Small 2018, 14, 1704282.
- [123] X. Wang, H. Zhang, H. Lin, S. Gupta, C. Wang, Z. Tao, H. Fu, T. Wang, J. Zheng, G. Wu, X. Li, *Nano Energy* **2016**, 25, 110.
- [124] D. Zhao, J. Shui, L. R. Grabstanowicz, C. Chen, S. M. Commet, T. Xu, J. Lu, D.

- Liu, Adv. Mater. 2014, 26, 1092.
- [125] W. Guo, X. Gao, M. Zhu, C. Xu, X. Zhu, X. Zhao, R. Sun, Z. Xue, J. Song, L. Tian, J. Xu, W. Chen, Y. Lin, Y. Li, H. Zhou, Y. Wu, *Energy Environ. Sci.* 2023, 16, 148.
- [126] Q. Wei, F. Xiong, S. Tan, L. Huang, E. H. Lan, B. Dunn, L. Mai, *Adv. Mater.* **2017**, *29*, 160230.
- [127] Z. Li, R. Gao, M. Feng, Y. Deng, D. Xiao, Y. Zheng, Z. Zhao, D. Luo, Y. Liu, Z. Zhang, D. Wang, Q. Li, H. Li, X. Wang, Z. Chen, *Adv. Energy Mater.* 2021, 11, 2003291
- [128] L. Gao, M. Xiao, Z. Jin, C. Liu, J. Ge, W. Xing, J. Energy Chem. 2019, 35, 17.
- [129] X. Lu, P. Yang, H. Xu, L. Xiao, L. Liu, R. Li, E. Alekseeva, J. Zhang, O. Levin, M. An, J. Mater. Chem. A 2023, 11, 3725.
- [130] H. S. Kim, J. Lee, J.-H. Jang, H. Jin, V. K. Paidi, S.-H. Lee, K.-S. Lee, P. Kim, S. J. Yoo, Appl. Surf. Sci. 2021, 563, 150208.
- [131] K. Ao, X. Zhang, R. R. Nazmutdinov, D. Wang, J. Shi, X. Yue, J. Sun, W. Schmickler, W. A. Daoud, *Energy Environ. Mater.* **2023**, e12499.
- [132] R. S. Varma, ACS Sustainable Chem. Eng. 2019, 7, 6458.
- [133] H. Xu, D. Wang, P. Yang, L. Du, X. Lu, R. Li, L. Liu, J. Zhang, M. An, *Appl. Catal. B: Environ.* **2022**, *305*, 121040.
- [134] G. Chen, P. Liu, Z. Liao, F. Sun, Y. He, H. Zhong, T. Zhang, E. Zschech, M. Chen, G. Wu, J. Zhang, X. Feng, *Adv. Mater.* **2020**, *32*, 1907399.
- [135] T. Wu, S. Li, S. Liu, W.-C. Cheong, C. Peng, K. Yao, Y. Li, J. Wang, B. Jiang, Z. Chen, Z. Chen, X. Wei, K. Wu, *Nano Res.* 2022, *15*, 3980.
- [136] J. Zhang, Q. Li, C. Zhang, L. Mai, M. Pan, S. Mu, *Electrochim. Acta* **2015**, *160*, 139.
- [137] C. Guo, W. Liao, Z. Li, C. Chen, *Carbon* **2015**, *85*, 279.
- [138] J. Zheng, C. Guo, C. Chen, M. Fan, J. Gong, Y. Zhang, T. Zhao, Y. Sun, X. Xu, M. Li, R. Wang, Z. Luo, C. Chen, *Electrochim. Acta* 2015, 168, 386.
- [139] M. Borghei, J. Lehtonen, L. Liu, O. J. Rojas, Adv. Mater. 2018, 30, 1703691.
- [140] X. Peng, L. Zhang, Z. Chen, L. Zhong, D. Zhao, X. Chi, X. Zhao, L. Li, X. Lu, K. Leng, C. Liu, W. Liu, W. Tang, K. P. Loh, Adv. Mater. 2019, 31, 1900341.
- [141] Y. Qian, Y. Li, Z. Pan, J. Tian, N. Lin, Y. Qian, Adv Funct Mater. 2021, 31, 2103115.
- [142] S. Zhang, W. Yang, Y. Liang, X. Yang, M. Cao, R. Cao, *Appl. Catal. B: Environ.* **2021**, 285, 119780.
- [143] J. Xie, B. Li, H. Peng, Y. Song, J. Li, Z. Zhang, Q. Zhang, *Angew. Chem. Int. Ed.* **2019**, *58*, 4963.
- [144] H. Yang, Y. Liu, X. Liu, X. Wang, H. Tian, G. I. N. Waterhouse, P. E. Kruger, S. G. Telfer, S. Ma, *eScience* **2022**, *2*, 227.
- [145] S. Gadipelli, T. Zhao, S.A. Shevlin, Z. Guo, Energy Environ. Sci. 2016, 9, 1661.
- [146] S. Gadipelli, Z. Li, T. Zhao, Y. Yang, T. Yildirim, Z. Guo, *J. Mater. Chem. A* **2017**, *5*, 24686.
- [147] J. Guo, Z. Li, G. He, H. Zhang, D. J. L. Brett, I. P. Parkin, Z. Guo, S. Gadipelli, Chem. Eng. J. 2024, 498, 155822.

- [148] J. Chen, J. Guo, H. Zhang, D. J. L. Brett, S. Gadipelli, *RSC Adv.* **2023**, *13*, 34556.
- [149] S. Gadipelli, Y. Lu, N. T. Skipper, T. Yildirim, Z. Guo, *J. Mater. Chem. A* **2017**, *5*, 17833.
- [150] T. Zhao, S. Gadipelli, G. He, M. J. Ward, D. Do, P. Zhang, Z. Guo, *ChemSusChem* **2018**, *11*, 1295.

Graphical Abstract



Highlights

- 1. Synthesis strategies for Fe₁-N_x-C electrocatalysts are insightfully presented.
- 2. Advancements in various forms of synthesis strategies are classified and summarized.
- 3. Advantages of hierarchical porous structures in zinc-air batteries are described.
- 4. Insights on the development of M₁-N_x-C catalysts for zinc-air battery are discussed.
- 5. Opportunities and challenges for rational design of Fe_1 - N_x -C catalysts are discussed.